11-10-2022

Post-wildfire Flood Inundation Modelling in Southern California: Implications for Dominant Processes and Parameter Identification

Francisca Olmos de Aguilera
Florida International University, folmo002@fiu.edu

FLORIDA INTERNATIONAL UNIVERSITY

Miami, Florida

POST-WILDFIRE FLOOD INUNDATION MODELLING IN SOUTHERN CALIFORNIA: IMPLICATIONS FOR DOMINANT PROCESSES AND PARAMETER IDENTIFICATION

A thesis submitted in partial fulfillment of the

requirements for the degree of

MASTER OF SCIENCE

in

ENVIRONMENTAL ENGINEERING

by

Francisca Olmos de Aguilera

2022

To: Dean John L. Volakis
College of Engineering and Computing

This thesis, written by Francisca Olmos de Aguilera, and entitled Post-wildfire Flood Inundation Modelling in Southern California: Implications for Dominant Processes and Parameter Identification, having been approved in respect to style and intellectual content, is referred to you for judgement.

We have read this thesis and recommend that it be approved.

_____

Ali Ebrahimian

_____

Arturo Leon

_____

Nawa Raj Pradhan

_____

Hector R. Fuentes, Major Professor

Date of Defense: November 10, 2022

The thesis of Francisca Olmos de Aguilera is approved.

_____

Dean John L. Volakis
College of Engineering and Computing

_____

Andrés G. Gil
Vice President for Research and Economic Development
and Dean of the University Graduate School

Florida International University, 2022

DEDICATION

This thesis is dedicated to my fiancé,

Alexander Loureiro,

for his love and unwavering support.

My parents,

Claudio Olmos de Aguilera

&

Paulina Besa

without them, the completion of this work would not be possible.

ACKNOWLEDGMENTS

I would like to acknowledge and extend my sincere gratitude to my major advisor, Dr. Hector R. Fuentes for his mentorship and support during my Master's program. His wisdom and passion in the field has inspired me and I could wholeheartedly say that I'd like to be in this field for the rest of my life. Thank you for your suggestions and constant support!

I would also like to thank my committee members, first, Dr. Nawa Raj Pradhan, without your expertise and guidance from the beginning, this thesis would not be possible. It has been a pleasure working with you virtually and in-person at CHL on this research. Furthermore, I would like to thank Dr. Ebrahimian and Dr. Leon for their knowledge and feedback in my thesis and master's coursework.

I would like to thank Dr. Ian Floyd for allowing me to join the wildfire flood risk management R&D efforts and his continued funding and support of my research over the years. Likewise, I would like to thank Joseph Sinicrope and Kiara Pazan for introducing me to ERDC and their encouragement and support over the years. I am forever grateful for the opportunities I have been given. Additionally, I wish to give a special thanks to my work colleagues, Taylor Cagle and Matthew Geheran who helped me throughout the thesis process.

This research was supported by the U.S. Army Corps of Engineers Engineering Research and Development Center. Thanks to their financial support, resources, and world-class engineers, I was able to complete my thesis.

ABSTRACT OF THE THESIS

POST-WILDFIRE FLOOD INUNDATION MODELLING IN SOUTHERN CALIFORNIA: IMPLICATIONS FOR DOMINANT PROCESSES AND PARAMETER IDENTIFICATION

by

Francisca Olmos de Aguilera

Florida International University, 2022

Miami, Florida

Professor Hector R. Fuentes, Major Professor

Wildfires produce large runoff volumes, sometimes in the form of debris flows (water-laden slurries of soil and rock that move rapidly through channels in steep landscapes) in response to moderate to severe precipitation events. For instance, in Santa Barbara and Ventura Counties following the 2017 Thomas Fire, on January 9th, 2018, an intense atmospheric river flood resulted in a series of destructive water and debris flows causing major damage to life and property. Inundation models that accurately parameterize and simulate hydrologic processes are in demand for post-wildfire flood susceptible regions like Southern California. This study utilizes the physics-based Gridded Surface Subsurface Hydrological Analysis, GSSHA, a fully coupled surface water/groundwater simulator with sediment transport capability, to simulate the flood event in the Santa Barbara watershed. The purpose of this study was to implement GSSHA to model pre- and post-fire conditions that allowed to locate dominant processes in relation to the model structure development for post-wildfire hydrologic modeling. A sensitivity analysis was performed using the SCE optimization algorithm.

Limitations in data due to the fire burning instrumentation equipment led to alternative techniques of parameterization. To reduce uncertainty, two methods of parameterization were applied: parameter transfer and optimization. It was found feasible to establish a transfer of parameters from a nearby, comparable watershed based on a previous study conducted by Pradhan and Floyd (2021). Subsequently, a sensitivity analysis was performed using the "Shuffled Complex Evolution" SCE optimization algorithm. The key parameters that were identified in the sensitivity analysis were manning's roughness and the hydraulic conductivity reduction factor. Although sensitive to both parameters, the model was found to be significantly more sensitive to the change in hydraulic conductivity reduction factor. Both types of parameterization found that post-fire simulations compared well to the observed data for the 09 January 2018 rainfall event. The post-wildfire numerical modeling approach provided an improvement to the existing state-of-practice for predicting post-wildfire inundation risks.

TABLE OF CONTENTS

CHAPTER PAGE

LIST OF TABLES

TABLE PAGE

LIST OF FIGURES

FIGURE PAGE

ABBREVIATIONS AND ACRONYMS

BAER	Burned Area Emergency Response
CD	Coefficient of Determination
CN	Curve Number
dNBR	Normalized Burn Ratio
ERDC	Engineering Research and Development Center
FEMA	Federal Emergency Management Agency
GLUE	Generalized Likelihood Uncertainty Estimator
GSSHA	Gridded Surface Subsurface Hydrologic Analysis
HEC-HMS	Hydrologic Modeling System
IDF	Intensity Duration Frequency
MTBS	Monitoring Trends in Burn Severity
NLCD	National Land Cover Database
NOAA	National Oceanic and Atmospheric Administration
NRCS	National Resource Conservation Service
PDS	Partial Duration Series
PF	Precipitation Frequency
RCS	Rowe Countryman and Storey
RF_k	Reduction Factor of Soil Hydraulic Conductivity
RMSE	Root Mean Square Error
SCE	Shuffled Complex Evolution
StreamStats	Streamflow Statistics and Spatial Analysis Tools
TR-55	Windows Technical Release 55

USACE	United States Army Corps of Engineers
USDA	United States Department of Agriculture
USGS	United States Geological Survey
WDTP	Water Drop Penetration Testing
WR	Water Repellency

1. INTRODUCTION

In recent decades, wildfires have increased in severity and frequency making it a major concern in the western US and other parts around the world. Post-wildfire storm events frequently create large runoff volumes, sometimes in the form of debris flows (water-laden slurries of soil and rock that move rapidly through channels in steep landscapes), that cause damage to life, property, and water supply (Cannon et al., 2008; Barnhart and Jones, 2021; Floyd, 2021). Predictions of post-wildfire flooding and debris flows are crucial to be prepared for emergency response after a wildfire. Currently, there is a demand for a physics-based hydrological framework that requires accurate parameterization of soil-hydraulic properties to reduce model uncertainty (Lane et al., 2006; Cannon and DeGraff, 2009; Moody, 2013). Southern California is a region in the US that can particularly benefit from improvements in post-wildfire model parametrization due to the frequency of wildfires in the area (Ebel and Moody, 2020). Wildfire in chaparral-vegetated basins affects hydrology, soil properties, and slope stability and causes an increase in the rate of sediment production and yield from hillslopes and in sediment yield from rivers (Florsheim et al., 1991; Scott and Williams, 1978; Rice, 1974). Uncertainty in future climate change, the existence of fire-prone vegetation along steep terrain and increasing human activity in the area all contribute to Southern California's predominantly high risks for post-wildfire floods and debris flows.

For example, the 2017 Thomas Fire, one of the largest fires in modern California history, demonstrated this need for readily available hazard assessment tools, after it burned 440 square miles through Santa Barbara and Ventura Counties. Following the fire, on January 9th, 2018, an intense atmospheric rainfall event occurred, triggering a series of destructive debris flows that

mobilized 680,000 m^3 of sediment in the Santa Ynes Mountains. This resulted in 23 fatalities, 167 injuries, 408 damaged homes, and $1.3 Billion in damages (Kean et al, 2019).

Before the debris-flow event, the best available predictions on potential inundation came from county, state, and federal floodplain maps (e.g., US Federal Emergency Management Agency [FEMA] 100-year floodplain). While valued, the floodplain maps do not account for fundamental differences in flow dynamics between water flows and debris flows (Kean et al, 2019). Hence, numerical modeling is a tool that can be used to predict post-wildfire inundation and debris flows. A numerical model that may support post-fire parametrization demands is U.S. Army Corps of Engineers (USACE) GSSHA, Gridded Surface Subsurface Hydrological Analysis, as it was designed to correctly identify and realistically simulate these two important hydrologic processes in watersheds (Downer and Ogden, 2006; Pradhan and Floyd, 2021). In this study, GSSHA was implemented to inform the potential for mitigation of the effects from inundation and debris-flow disasters in the future.

Parameters are part of a numerical model structure that are used to characterize the environment that is being simulated. For example, in a watershed model, it is important to have different parameters such as soil type, initial moisture content, and infiltration rates for accurately simulating surface runoff. By setting these parameters as closely as possible to what exists in the prototype, the model results are more likely to resemble events that occur in the real world. Poor identification of some of the parameters as well as errors in the model structure are the main contributors to the model uncertainty. Several watersheds around the world are either ungauged or poorly ungauged, therefore many regionalized studies provide a relationship between parameters of the model and the catchment descriptors so that parameters are transferable to similar regions (Pradhan et al., 2008). A proper and detailed analysis of the

parameters of a model and the model structure thereof can help estimate and reduce the uncertainties that can affect model predictions. To this end, a sensitivity analysis and estimation of predictive uncertainty have become central research topics in the hydrological modeling community (Abebe et al., 2010). The work by Spear and Hornberger (1980), the Generalized Likelihood Uncertainty Estimator (GLUE) approach of Beven and Binley (1992) and the Shuffled Complex Evolution (SCE) method of Duan et al. (1992) are among others for automatic calibration using optimization algorithms.

The purpose of this study was to implement GSSHA to model pre- and post-fire conditions that allowed to locate dominant processes in relation to the model structure development for post-wildfire hydrologic modeling. A sensitivity analysis was performed using the SCE optimization algorithm.

1.1 Objectives and Approach

The objectives of this research are to a) utilize GSSHA to model pre- and post-fire conditions, b) identify the most dominant parameters in relation to the model structure including relevant physical processes (i.e. change in surface roughness, infiltration, etc.) in post-wildfire hydrologic modelling, c) perform a sensitivity analysis and analyze and assess if optimized parameters and parameter dominance can be generalized. To reduce uncertainty, two methods of parameterization were applied: parameter transfer and optimization. First, a transfer of parameters of a nearby watershed with similar physical properties were used to simulate pre- and post- fire scenarios for the Santa Barbara watershed. Then, the SCE optimization algorithm was applied to calibrate a hydrologic parameter. By applying both methods of parameterization, generalization of the optimized parameter values were assessed by the validity of those parameter conditions in nearby watersheds under similar conditions.

1.2 Justification and Contribution

A limited understanding of physical processes involved in post-fire hydrology leaves fire-prone communities vulnerable to flooding and debris flows. The U.S. Army Corps of Engineers (USACE) Engineering Research and Development Center (ERDC) is developing new modeling techniques that accurately predict the areas at highest risk for deadly debris flows to be implemented across the United States. The USACE ERDC mission includes flood risk management, emergency management applications, and environmental concerns. This thesis will provide a guideline on GSSHA post-fire watershed hydrological model processes identification and parameterization in Southern California. A modelling procedure for post-fire flood inundation emergency assessments in the region will be implemented as a new reference for future modelling applications.

2. LITERATURE REVIEW

2.1 Post-fire Hydrology

Large, intense wildfires can significantly change the natural system and alter the land, hydrology, and ecology following the fire. Wildfires generate ash, decrease rainfall interception canopy, vegetation, and soil organic matter, and increase water-repellent soils (Ebel et al., 2012). These processes alter the soil profile and spatial variation of soil properties, increasing the potential for runoff and debris flows at watershed scales (Floyd, 2021). The limited understanding of physical processes coupled with sometimes inadequate availability of datasets (e.g, flow, depth, velocity) makes it difficult to accurately predict post-wildfire hydrographs (Moody et al., 2008a). The alteration of the soil structure in response to heating, burn severity, water repellency, and limitations in post-fire hydrology will be further discussed.

Soil properties located on or near the soil surface are more likely to be change by the fire as it is directly exposed. Consequently, organic matter and related soil properties are more likely to change than clay content which is concentrated in the subsurface layers (DeBano, 1991). Changes to the soil structure begin with vaporization of soil water at a temperature of 100^{o}C (Jian et al., 2018). Changes in soil organic matter start at 200^{o}C to 400^{o}C and changes of clay chemistry begin at 460^{o}C and end at 980^{o}C (DeBano, 1991). Mineral ash formations start from 500^{o}C to 1400^{o}C (Bodi et al., 2014). As a consequence of changes to the soil profile, affected environments may be subject to a range of hydrologic responses from no response to increased runoff and debris flows.

The term *burn severity* is largely based on loss of organic matter in the soil and on the soil surface organic matter conversion to ash. Remote sensing applications to assess burned areas typically use burn severity as a metric calculated from satellite sensors. Various remote sensing

data are used to generate an index known as Normalized Burn Ratio (dNBR), which is a preferable term as it separates the remote imaging index from surface measurements of the burned site (Keeley, 2009).Watersheds subjected to high severity burns, characterized by a deep ash layer, combustion of the organic forest floor, and charring of the organic matter in the soils, experience the most significant effects. (Miller, 1994; Martin and Moody, 2001).

Soil-water repellency or hydrophobic soil, when water does not immediately wet the soil, has been frequently observed after fires (Shilito et al., 2020). As discussed in Moody et al., (2013), "… no mathematical relations have been proposed to relate the degree of water repellency (WR) to runoff". The work by Shillito et al., (2020) addressed WR to relate to infiltration, a runoff generation process, for short precipitation events and dry conditions which are common after wildfires. The effective contact angle and soil-sorptivity, that captures water absorption by the soil as a function of surface tension and viscosity, was used to relate to infiltration. Validated by laboratory experiments using water drop penetration testing (WDTP) using silica sands, the results revealed that sorptivity was the highest for low effective contact angles (low water repellency) and decreased as the contact angle (water repellency) increased.

Few researchers have focused on predicting depth and downstream inundation and in developing fire-affected soil hydraulic functions (Elliot et al., 2010; Moody et al., 2013). The work by Pradhan and Floyd (2021) have articulated a formula that relates soil hydraulic conductivity to a burned severity factor to predict post-wildfire hydrologic response. In addition, post-wildfire flooding events are particularly difficult to quantify due to the intense erosion and deposition processes that often times damage or destroy instrumentation equipment (Moody et al., 2013). When data is insufficient, parameterization of physical processes can be achieved through auto-calibration and transferring parameters from a similar, nearby watershed to enhance

the process of predicting hydrologic response. This study simulated the 09 January 18 inundation and debris flow events documented in Kean et al., (2019) with auto-calibration and a transfer of parameters, and the addition of the soil hydraulic conductivity equation in Pradhan and Floyd (2021) to analyze and assess dominant and sensitive parameters.

2.2 Post-fire Study Models

After wildfires, the U.S. Department of Agriculture (USDA) and U.S. Department of the Interior assemble Burned Area Emergency Response (BAER) teams to immediately assess post-wildfire watershed conditions (Parsons et al., 2010). Several models and techniques have been available to predict post-fire runoff, varying from complexity and usability, and different modeling approaches may be suitable based on the watershed size. A survey on BAER models (Napper, 2010) found the five most common post-fire hydrologic models are: the Rowe Countryman and Storey (RCS), United States Geological Survey (USGS) Linear Regression Equations, USDA Windows Technical Release 55 (USDA TR-55), Wildcat5, and U.S. Army Corps of Engineers (USACE) Hydrologic Modeling System (HEC-HMS) (Kinoshita et al., 2014). Thus, highlighted are the contrasting models (empirical, semi-empirical, and semi-distributed), the lack of physics-based fully distributed models, and the need for systemic approaches in their application (i.e., parameterization, and adjusting for post-fire conditions).

One empirical model used in post-fire hydrology is the USGS Linear Regression Equation developed to estimate peak discharges (2 yr, 5 yr, 10 yr, 25 yr, 50 yr) for ungauged sites across the U.S. produced by using long-term discharge observations and the model summarizes physical basin characteristics (Kinoshita et al., 2014). It is an easy model to apply that requires few parameters but subject to large errors. Some of the semi-empirical approaches are the RCS, USDA TR-55, and Wildcat5. The RCS method estimates flood peaks and erosion

for basins specifically in Southern California (along the coast of the Mexican border to San Luis Obispo) (Rowe et al., 1949). Look up tables are used for pre- and post- fire flow and erosion rates and developed relations between storm precipitation and peak discharge frequencies for 256 watersheds within five zones. Although the RCS technique is practical with quick computation time, there are large inaccuracies for small watersheds and data is not regularly updated. Another semi-empirical model, TR-55, uses the Curve Number (CN) method that was developed by the USDA National Resource Conservation Service (NRCS) to predict runoff volume from agricultural settings (U.S. Department of Agriculture, Soil Conservation Service, 1991). The TR-55 models typically suitable for small urban and agricultural watersheds that accommodate three pre-defined rainfall distribution types using NRCS Type I, IA, II, and III. Wildcat5 is used extensively in U.S. Forest Service applications to wildland and runs interactively with spreadsheets (Microsoft Office Excel 2003 or later) using CN and its inputs include: storm characteristics, soil and land cover, timing parameters, and unit hydrograph selection. The outputs include a calculated hydrograph and peak runoff (Hawkins and Munoz, 2011).

Among semi-distributed models, HEC-HMS developed by the U.S. Army Corps of Engineers (USACE) is most commonly used in post-wildfire hydrology. CN is used for pre-fire conditions and post-fire CN assignment is based on expert's knowledge, because no specific guidelines are available to determine post-fire CN. The Green-Ampt (1911) infiltration model may also be used for soil parameters for pre- and post-fire conditions. The Muskingum-Cunge (Cunge, 1969) equation is used for routing open-channel flow (U.S. Army Corps of Engineers, 2010). Fully distributed models capture the spatial distribution of physical parameters including storm events, yet there are insufficient studies involved for post-fire hydrology. Similarly

developed by USACE, GSSHA (Gridded Surface Subsurface Hydrologic Analysis), is a distributed model that meets that need.

Hydrologic models are fundamental tools in the decision-making process for emergency response, yet, they were not designed for post-fire conditions, so they need to be adjusted accordingly (Zema, 2021). The BAER models are rarely evaluated under post-fire conditions (Chen et al., 2013). A better understanding of precipitation, infiltration, erosion, and runoff will lead to improved predictive modelling capabilities. The existing hydrological models should be specifically adapted to burned conditions with a reliable simulation of soil changes due to fire. Past models have limited their evaluations to existing models underburned and unburned conditions (Lopes et al., 2021). Therefore, there is a necessity for the development of fire-affected soil hydraulic functions and special conditions related to wildfires (Moody, 2013). Hydrologic models should include uncertainty analysis to provide a level of reliability and accuracy of their hydrological predictions.

2.2.1 Gridded Surface/Subsurface Hydrologic Analysis

Lumped parameter models normally use conceptual or empirical formulations for hydrologic processes and represent the watershed as a single homogeneous unit (Paudel et al, 2011). The main advantages of applying lumped models are that they are easy to use and are able to reproduce observed flows if given adequate calibration data. Over the past few years, physically-based distributed models have been developed and applied. These models distribute unit areas into grid cells and flows are routed from one grid cell to another as water drains through the basin (Jones, 1997). GSSHA (Gridded Surface Subsurface Hydrologic Analysis) is a physically-based, distributed watershed model that simulates event or continuous-based hydrologic responses.

GSSHA is a multidimensional modeling technology that couples overland, surface, and groundwater interactions to model Hortonian and Non-Hortonian flow. The model is intended to simulate different types of runoff production and determine the controlling physical processes in watersheds, i.e. infiltration excess, saturated source areas, and groundwater discharge. In addition, the model is to physically simulate soil erosion, transport and deposition, as well as constituent transport. GSSHA uses the diffusive wave equation from the Saint-Venant equations for one dimensional channel routing and two-dimensional overland flow routing. Green and Ampt and Richard's equations are incorporated to calculate infiltration soil parameters. It is a robust watershed modeling tool applicable for small and large watersheds as well as arid and humid environments.

2.3 Watershed Similarity

A watershed (or catchment) is defined as an area of land where water collects when it rains (drainage area), often bounded by its surface topography. Catchments are characterized by open systems with respect to input and output of fluxes of water and other quantities (Wagener et al., 2007; Dooge, 2003) and can be termed complex environmental systems. Progress in hydrology from empirical observations and classification to theorizing has been really slow due to the fact that all places are unique. Beven (2000a) discusses the uniqueness of a place in their characteristic of topography, soil, rocks, vegetation, and anthropogenic modification. Simulation models can provide a better understanding of extrapolating knowledge watershed to watershed, particularly a site where no data are available. The uniqueness of the catchment will be reflected in the parameter values that represent it. Winter (2001) suggests that areas that have similar land slopes, surficial geology, and climate will result in similar hydrologic flow paths regardless of the geographic location of the site. The complexity and differences between watersheds can lead

to advancements in hydrologic science through the formulation of hypothesis or relationships that may have general applicability. In this study, a transfer of parameters between watersheds is applied to enhance simulations due to a lack of data. To reduce uncertainty, redundancy is established in this study with the addition of transferred parameters and auto-calibration.

2.4 Study Area

The impacted watershed analyzed in this study was San Ysidro Creek located in Southern California. The watershed spans the peaks of California's Transverse Ranges, exceeding 1,100 m in elevation and drain into the Pacific Ocean. The climate type is Mediterranean with dry, warm summers and wet, cool winters where precipitation occurs mostly as rain. The vegetation type is 54% mixed chaparral consisting of chamise (Adenostoma fasciculatum), chaparral whitehorn (Ceanothus leucodermis), and manzanita (Arctostaphylos manzanita). Geology within the burn area is primarily sedimentary in origin, consisting of older Cretaceous to Miocene age strata to the north and late Miocene to Pleistocene age strata to the south. There are approximately 170 soil types that are identified within the Thomas Fire burn area (State of California, 2018). Maximum rainfall intensities were reported on January 9, 2018 with 6.48 in hr^{-1} (165 mm hr^{-1}) for the 5-minute duration rainfall, and 3.44 in hr^{-1} (87 mm hr^{-1}) for the 15-minute duration rainfall.

On 4 December 2017, the Thomas Fire ignited, close to Thomas Aquinas College, from which the fire derived its name. A total of 282,000 acres burned breaking through Santa Barbara and Ventura Counties, with full containment not declared until 12 January 2018 (Figure 1). Burn severity analyses of satellite coverage data showed that 11% of the area within the burn boundary were unburned, 31% burned with low severity, 56% moderately burned, and a final 1% burned with high severity (Addison and Oommen 2019). On 9 January 2018, intense rainfall on

the recently burned mountain terrain caused a series of debris flows to surge downstream from the Santa Ynes Mountains (Floyd, 2021). This study demonstrates the results from hydrologic modeling of San Ysidro Creek (Figure 2).

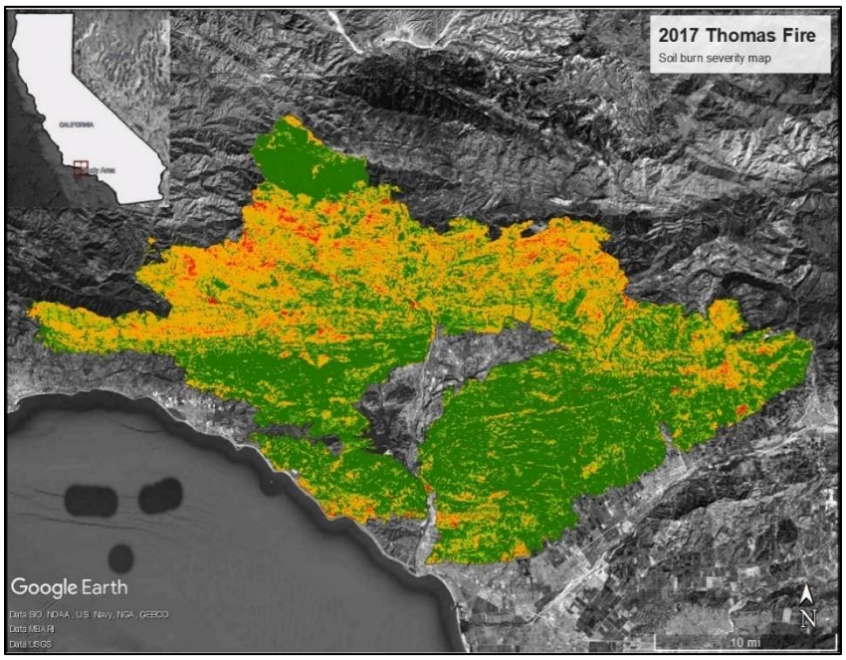

Figure 1. Burn severity Map of 2017 Thomas Fire perimeter affecting Santa Barbara and Ventura Counties, CA (Red represents high burn, orange is medium burn, and green is low burn). Amended map provided by the USDA Forest Service, Geospatial Technology and Applications Center, BAER Imagery Support Program: (Source: https://burnseverity.cr.usgs.gov/baer/baer-imagery-support-data-download).

Figure 2. Resulting debris flows of post-wildfire impacted watershed in Santa Barbara (Montecito Creek, and San Ysidro Creek shown in red).

3. METHODOLOGY

Intense wildfires reduce vegetation canopy and catalyze several changes to soil properties that vary spatially and alter the soil profile (Moody, 2013). Infiltration rates are a function of various factors where hydraulic conductivity plays a critical role (Ebrahimian et al., 2019). Water distribution and flow in the vadose zone, are strongly influenced by the intrinsic properties of the soil matrix (John and Fuentes, 2021). Chemical and physical changes to the soil structure affect infiltration and hydraulic conductivity, and a reduction in vegetation affects surface roughness. Accordingly, a sensitivity analysis of hydraulic conductivity and surface roughness using GSSHA were analyzed using the SCE optimization algorithm and the identification of the model parameters were analyzed in relation to model structure development for post-wildfire hydrology.

GSSHA represents a fully coupled surface water/groundwater simulator with sediment transport capability. The model can simulate different types of runoff generation mechanisms including the infiltration excess mechanism defined by Richards' equation and the Green and

Ampt method (1911). Numerous free surface flows are unsteady and non-uniform where spatial and temporal changes of water stages and flow discharges need to be determined (Leon, 2013). Channel routing in GSSHA uses an explicit solution of the diffusive wave equation (Julien and Saghafian 1995). Recent developments in GSSHA also include post-wildfire runoff generation mechanisms. In addition, the model has a robust transport mechanism that includes runoff routing coupled with soil erosion, transport, and deposition. This study included runoff generation and routing mechanisms in the model development process as well as the model's structural and parametric analysis process.

At times, numerical models contain parameters that cannot be measured directly but only be inferred by a calibration process that adjusts values to match the model to the real system it represents (Abebe et al., 2010; Madsen, 2000). Traditional calibration procedures are labor intensive and involve frequent manual adjustments. Therefore, automatic methods for model calibration have become a common practice. A powerful, efficient procedure is the Shuffled Complex Evolution (SCE) method, a global optimization algorithm, initially developed by Duan et al. (1992). Various case studies have demonstrated that the SCE algorithm is consistent and efficient in locating optimal model parameters of a hydrological model (Vrugt and Bouten, 2003). SCE is based on four concepts: (1) combination of probabilistic and deterministic approaches; (2) clustering- shuffling of complexes and information sharing; (3) systematic evolution of a complex of points spanning the space, in the direction of global improvement; and (4) competitive complex evolution (Duan et al., 1992).

3.1 Hydrologic Processes

Understanding hydrologic processes of a watershed is not possible with only rainfall (input) and discharge (output) data as many processes may lead to comparable hydrographs. Rainfall

and discharge, alone, do not provide adequate information of hydrologic response. Therefore, the identification of runoff generation and routing processes requires further investigation within the catchment basin to accurately characterize dominant water flow pathways (Latron and Gallart, 2008). In this study, runoff generation and routing processes are examined.

3.1.1 Runoff Generation

Runoff occurs due to excess precipitation that flows until it reaches streams, rivers, and oceans and varies within time and space. Critical controls for runoff generation are precipitation intensity, duration of precipitation, and infiltration/storage capacity of the soil (Thompson et al, 2011; Tindall and Kunkel, 1999). Following a high intensity wildfire, runoff can significantly increase through a loss of vegetation precipitation interception canopy (Floyd, 2021). Wildfires change infiltration soil properties, sometimes making the soil hydrophobic (water-repellent). Therefore, it is critical to observe infiltration and how it relates to changes in burn conditions.

3.1.1.1 Infiltration

Infiltration is the process whereby rainfall and ponded surface water seep into the soil due to gravity and capillary suction. Green and Ampt (1911) developed a simple infiltration model that is theoretically based on Darcy's Law with physically significant parameters that can be computed from soil properties. Water is assumed to enter the soil as a sharp wetting front. Precipitation on initially dry soil quickly infiltrates due to capillary pressure and as rainfall continues, the ground becomes saturated and the infiltration rate will decrease until it approaches the saturated hydraulic conductivity of the soil. Infiltration rate is a function of hydraulic conductivity, pressure head, total porosity, effective porosity and saturation, and cumulative infiltration depth and is expressed as:

$$f(t) = K\left[\frac{h_p \Delta p_0}{F(t)} + 1\right] \quad (1)$$

Where: $f(t)$ = infiltration rate at time t

K = hydraulic conductivity

H_p = pressure head for wetting at the wetting front

P_o = total porosity

P_{oi} = initial water content

P_{or} = residual water content

$P_{oe} = p_o - p_{or}$ = effective porosity

$S_e = p_{oi}/p_{oe}$ = Effective saturation

$\Delta p_o = p_o - p_{oi} = p_{oe} - S_e p_{oe} = (1 - S_e)p_{oe}$ = change in total porosity

F(t) = cumulative infiltration depth at time t

3.1.1.2 Post-fire Condition

Accounting for changes in infiltration with changing burn severities is valuable for accurately predicting hydrological response. Pradhan and Floyd (2021) developed a post-fire condition formulation that includes multiplying factors, based on the physics based Green & Ampt distributed vadose zone infiltration process, which are explicitly linked to burned severities, to reduce an unburned soil hydraulic conductivity. Accordingly, the multiplying factors incorporate soil hydraulic conductivity reduction factor, and burned severity factor as follows:

$$k_{burned} = RF_k \cdot BDF \cdot k_{unburned} \quad (2)$$

Where: k_{burned} = soil hydraulic conductivity at burned condition

RF_k = Reduction Factor of soil hydraulic conductivity under burned condition

BDF = Burn Degree Factor

$k_{unburned}$ = soil hydraulic conductivity at normal unburned condition

In calibration, the reduction factor (RF_k) was considered from 0.05 to 0.90 (95% to 10% reduction range).

3.1.2 Routing

Routing is essential in estimating the propagation of flood from upstream to the downstream of a river, lakes, and reservoirs. Understanding routing processes can help predict the hydrograph shape following rainfall events in a watershed. Hydraulic or distributed routing is based on the solution of partial differential equations of unsteady open-channel flow, and the equations used are the Saint-Venant equations. The hydraulic models require gathering a lot of data to solve the equations numerically. GSSHA uses the diffusive wave equation to model 1-D channel and 2-D overland flow routing and requires surface roughness to be applied at every cell grid to relate to flow rate.

3.1.2.1 Diffusive Wave

Channel routing in GSSHA is simulated using an explicit solution of the diffusive wave approximation from the Saint-Venant Equations which combines the continuity and momentum equations. Since it is a non-linear equation, it requires numerical methods and large quantities of

measured data. The diffusive wave is valid when the inertial acceleration is less than gravity, friction, and pressure terms, primarily where there is subcritical flows, with low Froude values:

Continuity

Conservation form $$\frac{\partial Q}{\partial x} + \frac{\partial A}{\partial x} = 0 \quad (3)$$

Momentum

Conservation form $$\frac{1}{A}\frac{\partial Q}{\partial t} + \frac{1}{A}\frac{\partial}{\partial x}\left(\frac{Q^2}{A}\right) + \frac{\partial y}{\partial x} - g\left(S_0 - S_f\right) = 0 \quad (4)$$

The diffusive wave model (also known as the non-inertia model) is written as:

$$g\frac{\partial y}{\partial x} - g\left(S_0 - S_f\right) = 0 \quad (5)$$

Where: x = longitudinal distance along the channel or river

y = depth of flow

g = acceleration due to gravity

S_0 = channel bottom slope

S_f = friction slope

3.1.2.2 Surface Roughness

Water on the soil surface that neither infiltrates nor evaporates will pond on the surface, it can also move from one grid cell to the next as overland flow. Overland flow in GSSHA employs the same methods described for 1-D channel routing, except with calculations made in

two dimensions. Numerical models such as GSSHA implement Manning's equation to relate surface roughness to flow rate:

$$Q = \frac{1}{n} A R^{\frac{2}{3}} S_f^{\frac{1}{2}} \quad (6)$$

Where: A = channel flow cross sectional Area

P = wetted perimeter

R = $\frac{A}{P}$ = hydraulic radius

S_f = friction slope

n = Manning's roughness coefficient

Surface roughness is an important parameter as it controls runoff on hillslopes and in channels through the frictional resistance parameter (Moody et al., 2013).

3.2 Parameterization

Providing adequate information of the physical processes of a system to model and defining parameter values for a hydrologic model application (i.e., parameterization) are crucial and difficult tasks. Generally model applications use a combination of measured, estimated, and optimized parameter values (Malone et al., 2015). Parameterization is critical in order to avoid methodological problems at the subsequent phases of model calibration and validation. According to Refsgaard and Storm (1996), parameter values should be defined from as much available field data as possible, for the parameters subject to calibration physically acceptable ranges should be estimated, and the number of calibrated parameters should be kept low.

In lumped conceptual models, parameters do not have a physical meaning, therefore parametrization is not restricted to physical boundaries. By definition, a distributed physically based model, such as GSSHA, contains parameters that can be assessed from field measurements and do not require calibration if there is sufficient data (Feyen et al, 2000). Due to the Thomas

wildfire following intense rainfall, parameters were not directly assessed and therefore require calibration. Fortunately, a similar study has been assessed in a nearby watershed in southern California (Pradhan and Floyd, 2021) and so parameters can be transferred accordingly. For redundancy, the two methods of parameterization in this study are parameter transfer and optimization.

3.2.1 Parameter Transfer

The Santa Barbara watershed were modeled after the Arroyo Seco watershed due to its proximity and similarities (Pradhan and Floyd, 2021). Geographic coordinates of the watersheds are shown in Table 1. The watershed is located in Southern California, 82 miles away from the Santa Barbara watershed (Figure 3) and is part of the Transverse Range. Both studies (Arroyo Seco and San Ysidro Creek) were based on event-based simulations.

Table 1.Geographic coordinates for each watershed.

Watershed	Latitude	Longitude
San Ysidro Creek	34º29’08” North	119º36’03” West
Arroyo Seco	34º13’20” North	118º10’36” West

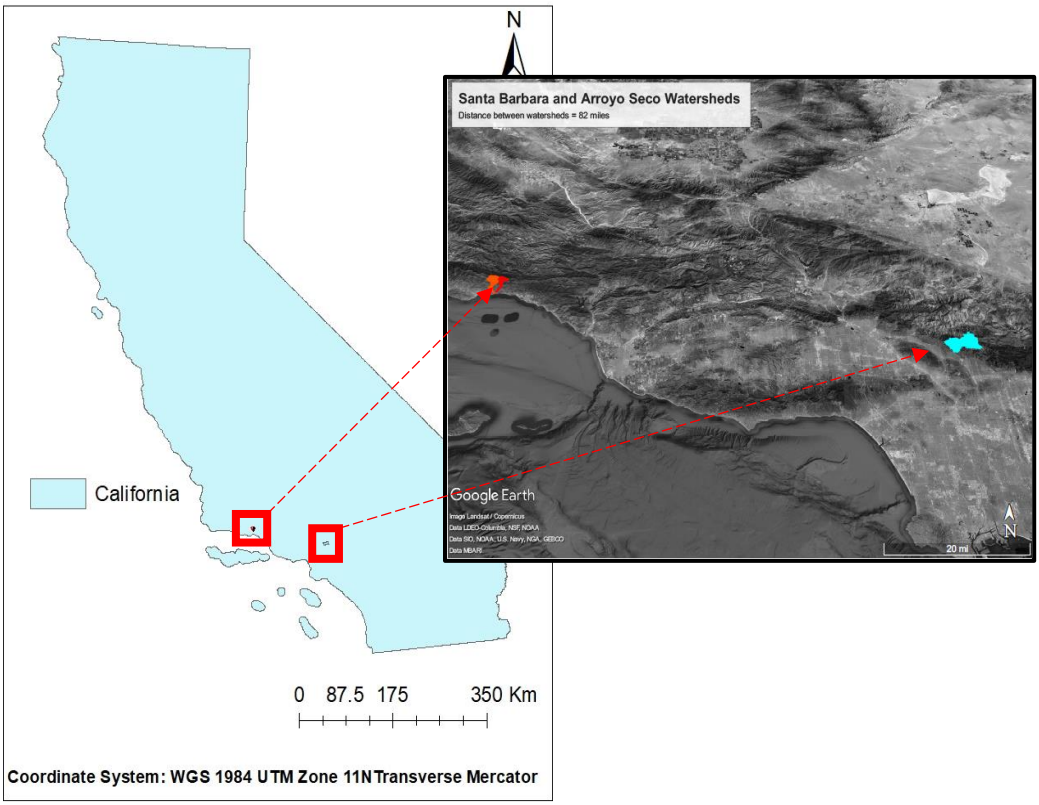

Figure 3. Distance between San Ysidro and Arroyo Seco watersheds located in Southern California.

The Arroyo Seco watershed was calibrated using the 2008 National Land Cover Database (NLCD) prior to the fire (Figure 4). According to the 2008 NLCD, San Ysidro Creek had a similar land use type for the burned portion of the watershed (Figure 5). The San Ysidro Creek southern portion was not burned and mostly residential, developed land. Otherwise, the majority of the area was 19.81% shrub/scrub, 30.98% mixed forest, and 28.14% evergreen forest. Arroyo Seco had a majority land use type of 56.52% shrub/scrub, 35.50% evergreen forest, and 4.99% mixed forest. The Arroyo Seco watershed is closer north of the Transverse range, while San

Ysidro is closer to the coast and for this reason there is more developed land.

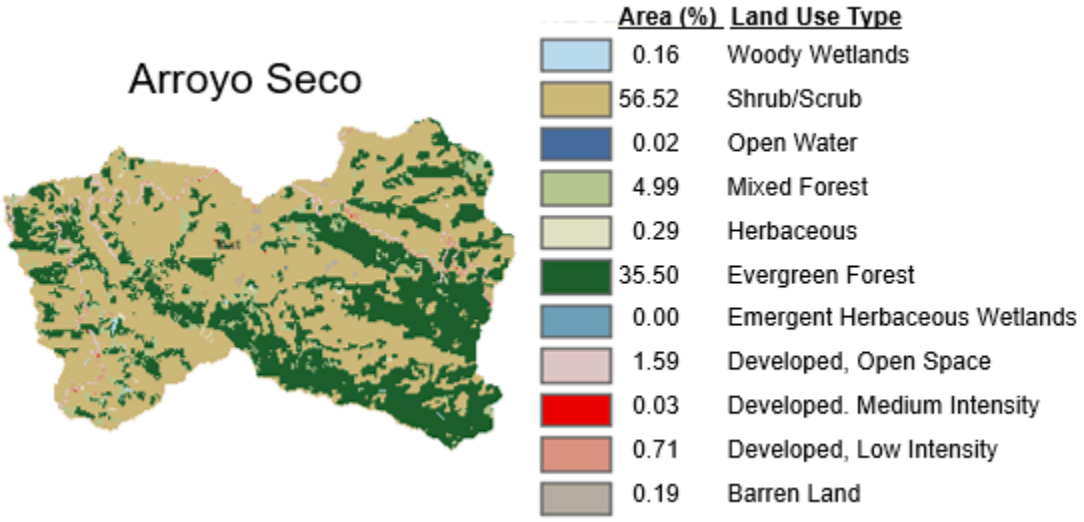

Figure 4. Arroyo Seco land use from 2008 NLCD. (Source: http://www.mrlc.gov/).

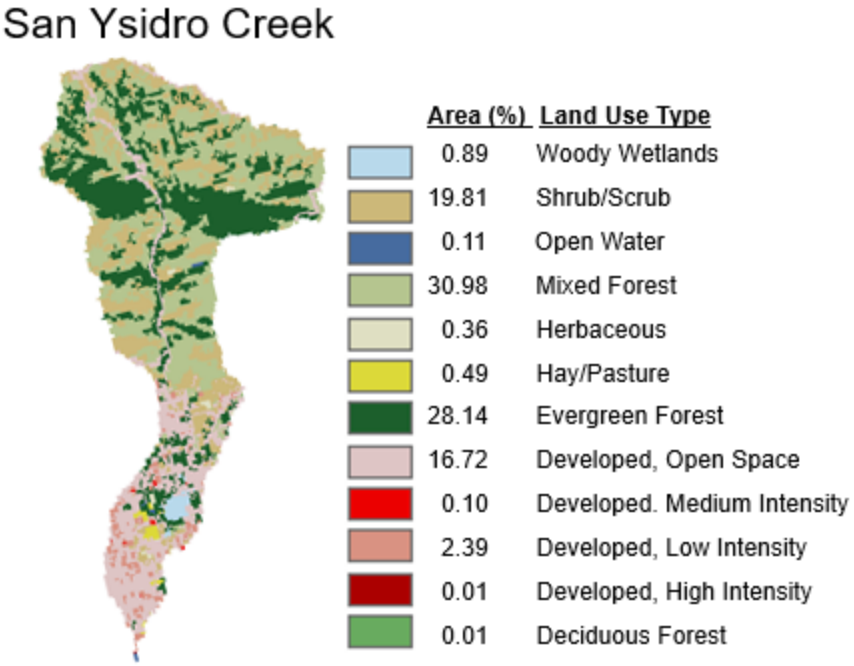

Figure 5. San Ysidro Creek land use from 2008 NLCD. (Source: http://www.mrlc.gov/).

3.2.2 Optimization

Optimization or auto-calibration finds the best solutions with regard to some conditions. There are three components to optimization; (1) an objective function that mathematically minimizes or maximizes a numeric value and indicates a goodness of fit measure, (2) decision variables are assigned that correspond to the options available to be manipulated, and (3) constraints, requirements imposed on the options. To apply hydrological optimization, a simulation is run to find constraint coefficients for the optimization. A cost function can be added with a set of possible decisions, and solve the optimization model to find the best solution.

Performance evaluation in the calibration and validation process can be evaluated both qualitatively, visually, and quantitatively, with statistical measures. Both methods were applied in this study, the first of which included a visual inspection of the model, then statistical criteria used in the analysis (Feyen et al, 2000). The statistical criteria used in the analysis are the objective functions: the Coefficient of Determination (CD), R^2, and the Root Mean Square Error (RMSE).

These measures are given as:

$$R^2 = \frac{\sum_{i=1}^{n}[O_i - S_i]^2}{\sum_{i=1}^{n}[O_i - \bar{O}_i]^2} \tag{7}$$

$$RMSE = \sqrt{\frac{\sum_{i=1}^{n}[O_i - S_i]^2}{n}} \tag{8}$$

Where $O_{,i}$ is the i-th observed value , $S_{,i}$ is the i-th simulated value, $\bar{O}_i$ is the average of the observed values, and n is the number of observations in the considered period.

The CD describes the ratio of scatter plot of the simulated and observed values around the average of the observations. A CD value of one shows that the simulated and observed values

match completely; the minimum value is zero and is positive. The RMSE provides a good measure of the average difference between the observed and simulated values, and can be positive or negative (Feyen et al, 2000). A perfect fit is typically indicated by values close to zero.

Figure 6 summarizes the SCE optimization algorithm process in a flow chart. First, parameters are defined for the simulation, observed data is considered from boundary conditions and rain gages. The algorithm generates a random population with selected parameters, uses the objective function, then the evolution process begins with multiple GSSHA simulations. A test for convergence will then provide inundation depths and optimized parameters. If there is no convergence, the evolution process needs to be repeated.

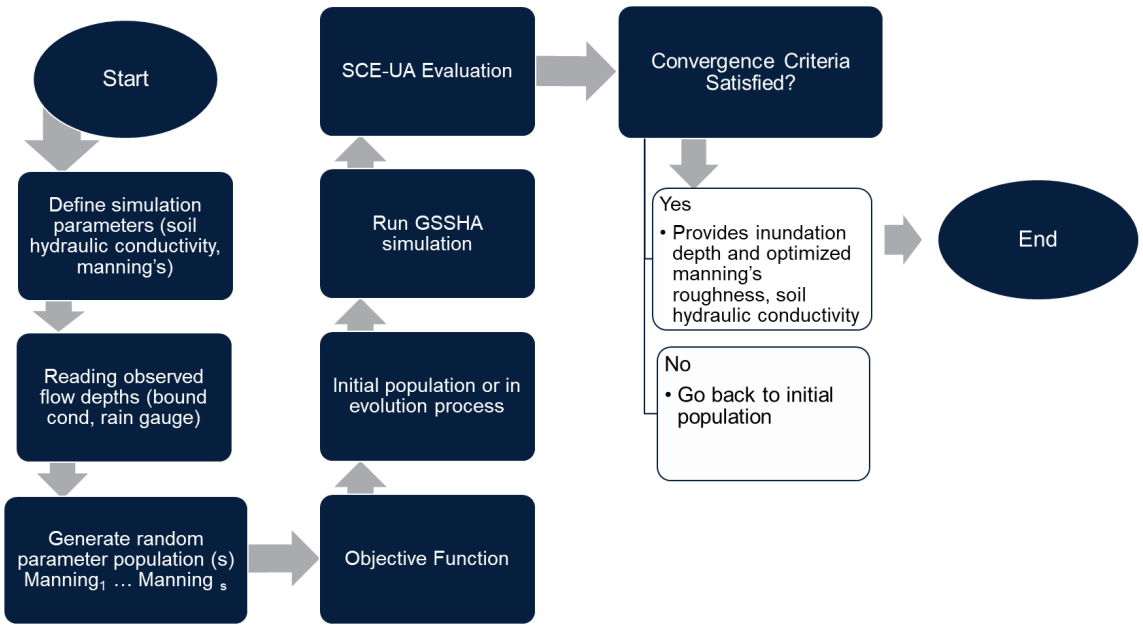

Figure 6. Flowchart on optimization process.

3.3 Input Data

Necessary data required data for GSSHA to run simulations included the observed maximum flow depths, precipitation data, the extent of the watershed, land cover and burn severity maps, and the parametric values. Table 2 summarizes the data type, source, and format used to support the GSSHA model.

Table 2. Summary of Data, Source, and Format.

Data Type	Source	Format
Maximum Flow Depths	Kean et al. (2019), USACE LA District	Shapefile
Precipitation	County of Santa Barbara	Spreadsheet, Appendix A
Watershed Extent	USGS Stream Stats	Shapefile
Land Cover	2016 USGS National Land Cover Database (NLCD)	Raster, Appendix C
Burn Severity	Monitoring Trends in Burn Severity (MTBS)	Raster, Appendix E
Parametric values (e.g. hydraulic conductivity, manning's roughness, etc.)	Pradhan and Floyd (2021)	Appendix B,C,D,E

3.3.1 Maximum Flow Depth

Data from Kean et al. (2019) provided maximum flow depth, h, from the flood event mudlines on trees and infrastructure across the inundation areas from the 2018 debris flow event shown in Figure 7. High-resolution satellite imagery was used to precisely map the inundation boundary. The inundation extents derived from Kean et al. (2019) were acquired from the USACE Los Angeles District. These datasets provide the basis for model validation.

Figure 7. Maximum flow depth values on map of watershed.

3.3.2 Precipitation

Incremental totals for 2018 January 9 precipitation event was obtained from the County of Santa Barbara's automated sensors at 5-minute intervals. Substantial rainfall rates were reported to be 165 mm hr^{-1} for 5-min intensity and 87 mm hr^{-1} for 15-min intensity (State of California, 2018). The County of Santa Barbara provides this data at (https://rain.cosbpw.net/). The precipitation dataset was interpolated from stations within the watershed using the inverse distance weighting (IDW) interpolation shown in Table 3. The rainfall data was used for calibration, parameter identification and verification of the post-fire watershed hydrological model.

Table 3. Coordinates of Precipitation Station Gauges. (Source: State of California, 2018).

Gauge	Longitude	Latitude
Summerland	119.5814 °W	34.4153 °N
Montecito	119.6404 °W	34.4275 °N
Doulton Tunnel	119.5658 °W	34.4578 °N

3.3.2.1 Return Period

The Montecito Water District station located in Santa Barbara, CA (Latitude: 34.4333°, Longitude:-119.6333°), elevation: 230ft, shown in Figure 8, was used to demonstrate the return period range. The rainfall intensity had a 0.2% to 0.5% annual percent chance exceedance.

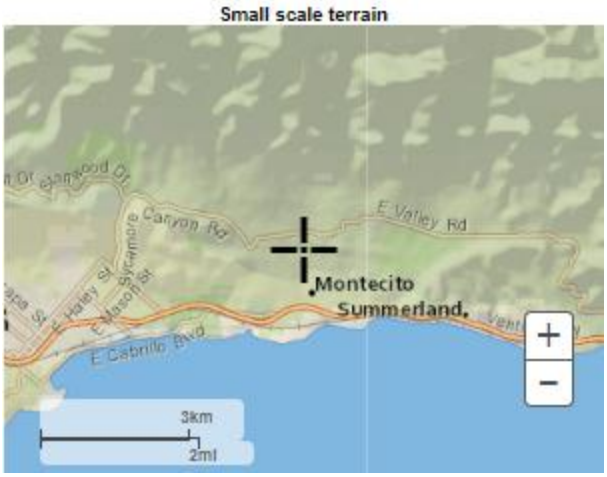

Figure 8. Montecito Water District station location.

Precipitation frequency (PF) estimates based on frequency analysis of partial duration series (PDS) were found from the National Weather Service's National Oceanic and Atmospheric Administration Atlas 14 (NOAA Atlas 14) Volume 1. The 0.2 to 0.5% annual percent exceedance corresponds to a 200 to 500-year return period or recurrence interval in a 5-minute duration with estimates of 6.01 to 6.74 in per hour, as shown in Table 4.

Table 4. Precipitation Frequency Estimates in Inches.

PF tabular

PDS-based point precipitation frequency estimates with 90% confidence intervals (in inches/hour)[1]

Duration	Average recurrence interval (years)									
	1	2	5	10	25	50	100	200	500	1000
5-min	1.92 (1.64-2.26)	2.45 (2.09-2.88)	3.12 (2.65-3.70)	3.66 (3.08-4.38)	4.38 (3.54-5.46)	4.92 (3.89-6.29)	5.46 (4.19-7.20)	6.01 (4.45-8.20)	6.74 (4.75-9.66)	7.30 (4.94-10.9)
10-min	1.37 (1.18-1.62)	1.75 (1.50-2.07)	2.23 (1.90-2.65)	2.62 (2.21-3.14)	3.14 (2.54-3.91)	3.52 (2.78-4.51)	3.91 (3.00-5.15)	4.31 (3.19-5.87)	4.83 (3.41-6.92)	5.23 (3.54-7.81)
15-min	1.11 (0.948-1.31)	1.41 (1.21-1.67)	1.80 (1.54-2.13)	2.11 (1.78-2.53)	2.53 (2.05-3.15)	2.84 (2.24-3.64)	3.16 (2.42-4.16)	3.47 (2.57-4.73)	3.90 (2.75-5.58)	4.22 (2.86-6.30)
30-min	0.858 (0.736-1.01)	1.09 (0.936-1.29)	1.40 (1.19-1.65)	1.64 (1.38-1.96)	1.96 (1.59-2.44)	2.20 (1.74-2.82)	2.45 (1.88-3.22)	2.69 (2.00-3.67)	3.02 (2.13-4.33)	3.27 (2.21-4.88)
60-min	0.646 (0.553-0.762)	0.823 (0.704-0.972)	1.05 (0.895-1.24)	1.23 (1.04-1.48)	1.47 (1.20-1.84)	1.66 (1.31-2.12)	1.84 (1.41-2.42)	2.03 (1.50-2.76)	2.27 (1.60-3.25)	2.46 (1.66-3.67)
2-hr	0.474 (0.406-0.559)	0.604 (0.517-0.714)	0.772 (0.658-0.914)	0.906 (0.764-1.08)	1.08 (0.878-1.35)	1.22 (0.962-1.56)	1.35 (1.04-1.78)	1.49 (1.10-2.03)	1.67 (1.18-2.40)	1.81 (1.23-2.70)
3-hr	0.391 (0.335-0.462)	0.499 (0.427-0.589)	0.637 (0.543-0.755)	0.747 (0.631-0.894)	0.894 (0.724-1.12)	1.00 (0.793-1.29)	1.12 (0.855-1.47)	1.23 (0.909-1.67)	1.38 (0.970-1.97)	1.49 (1.01-2.22)
6-hr	0.285 (0.244-0.336)	0.363 (0.311-0.429)	0.463 (0.395-0.549)	0.543 (0.458-0.650)	0.648 (0.525-0.808)	0.727 (0.574-0.930)	0.806 (0.618-1.06)	0.885 (0.656-1.21)	0.990 (0.698-1.42)	1.07 (0.724-1.60)
12-hr	0.186 (0.159-0.219)	0.238 (0.203-0.280)	0.303 (0.258-0.358)	0.354 (0.299-0.423)	0.421 (0.341-0.525)	0.470 (0.372-0.602)	0.519 (0.398-0.684)	0.568 (0.421-0.774)	0.632 (0.446-0.906)	0.680 (0.460-1.01)
24-hr	0.122 (0.106-0.143)	0.156 (0.136-0.183)	0.200 (0.173-0.235)	0.234 (0.202-0.277)	0.278 (0.233-0.340)	0.311 (0.255-0.387)	0.343 (0.275-0.437)	0.375 (0.293-0.490)	0.417 (0.313-0.566)	0.448 (0.326-0.628)
2-day	0.075 (0.065-0.088)	0.098 (0.085-0.115)	0.128 (0.111-0.150)	0.151 (0.130-0.179)	0.182 (0.152-0.223)	0.206 (0.169-0.256)	0.229 (0.184-0.292)	0.253 (0.198-0.331)	0.284 (0.214-0.386)	0.308 (0.224-0.432)
3-day	0.056 (0.048-0.065)	0.074 (0.064-0.086)	0.097 (0.084-0.114)	0.116 (0.100-0.137)	0.142 (0.118-0.173)	0.161 (0.132-0.201)	0.181 (0.145-0.231)	0.202 (0.158-0.264)	0.229 (0.172-0.311)	0.251 (0.183-0.352)
4-day	0.044 (0.039-0.052)	0.059 (0.051-0.069)	0.079 (0.068-0.092)	0.095 (0.081-0.112)	0.116 (0.097-0.142)	0.133 (0.109-0.166)	0.151 (0.121-0.192)	0.169 (0.132-0.220)	0.193 (0.145-0.263)	0.213 (0.155-0.298)
7-day	0.030 (0.026-0.035)	0.039 (0.034-0.046)	0.053 (0.046-0.062)	0.064 (0.055-0.076)	0.080 (0.067-0.097)	0.092 (0.076-0.115)	0.105 (0.085-0.134)	0.119 (0.093-0.156)	0.139 (0.105-0.189)	0.155 (0.113-0.217)
10-day	0.022 (0.019-0.026)	0.030 (0.026-0.035)	0.040 (0.034-0.047)	0.048 (0.042-0.057)	0.061 (0.051-0.074)	0.071 (0.058-0.088)	0.081 (0.065-0.104)	0.093 (0.073-0.121)	0.109 (0.082-0.148)	0.122 (0.089-0.172)
20-day	0.013 (0.011-0.015)	0.017 (0.015-0.020)	0.024 (0.021-0.028)	0.029 (0.025-0.035)	0.037 (0.031-0.045)	0.043 (0.036-0.054)	0.050 (0.040-0.064)	0.058 (0.045-0.076)	0.069 (0.052-0.094)	0.078 (0.057-0.110)
30-day	0.010 (0.009-0.012)	0.014 (0.012-0.016)	0.019 (0.016-0.022)	0.023 (0.020-0.027)	0.029 (0.025-0.036)	0.035 (0.028-0.043)	0.040 (0.032-0.051)	0.046 (0.036-0.061)	0.055 (0.042-0.075)	0.063 (0.046-0.088)
45-day	0.008 (0.007-0.010)	0.011 (0.010-0.013)	0.015 (0.013-0.018)	0.018 (0.016-0.022)	0.024 (0.020-0.029)	0.028 (0.023-0.035)	0.032 (0.026-0.041)	0.037 (0.029-0.049)	0.044 (0.033-0.060)	0.050 (0.037-0.070)
60-day	0.007 (0.006-0.008)	0.009 (0.008-0.011)	0.013 (0.011-0.015)	0.016 (0.014-0.019)	0.020 (0.017-0.024)	0.023 (0.019-0.029)	0.027 (0.022-0.035)	0.031 (0.024-0.041)	0.037 (0.028-0.050)	0.042 (0.031-0.059)

[1] Precipitation frequency (PF) estimates in this table are based on frequency analysis of partial duration series (PDS).

Numbers in parenthesis are PF estimates at lower and upper bounds of the 90% confidence interval. The probability that precipitation frequency estimates (for a given duration and average recurrence interval) will be greater than the upper bound (or less than the lower bound) is 5%. Estimates at upper bounds are not checked against probable maximum precipitation (PMP) estimates and may be higher than currently valid PMP values.

Please refer to NOAA Atlas 14 document for more information.

Similarly, Figure 9 demonstrates the light blue as 200-year and cyan as the 500-year return periods categorized by different durations in the PDS-based intensity-duration-frequency (IDF) curves.

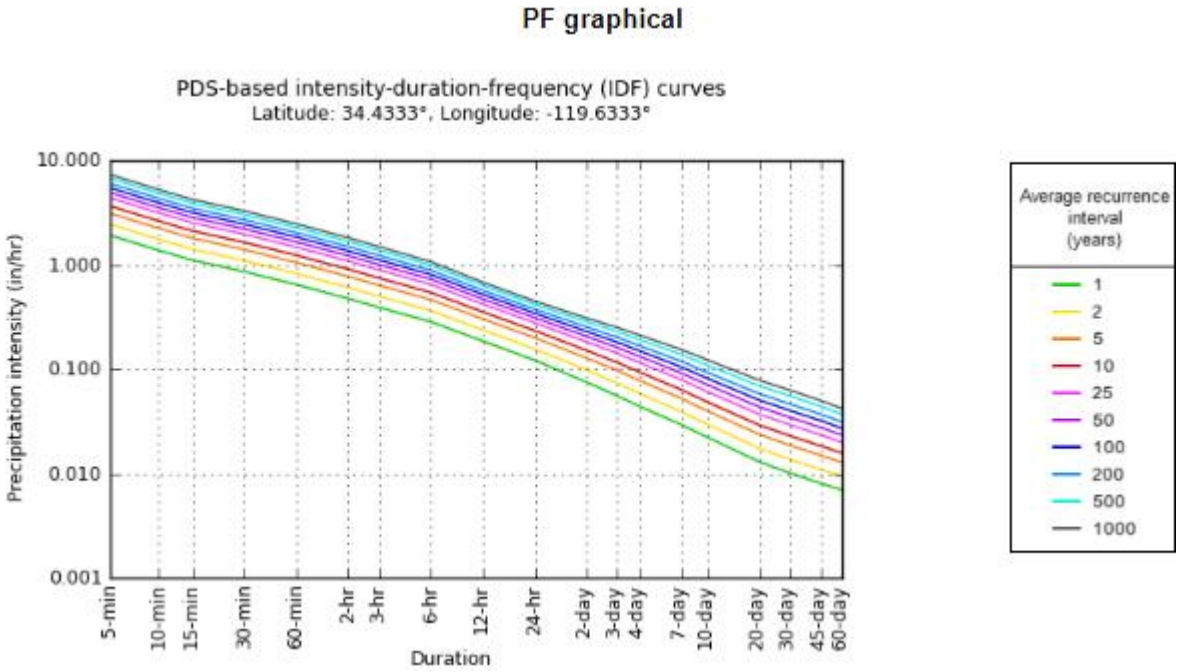

Figure 9. Graphical representation of precipitation frequency.

3.3.3 Watershed Extent, Land Cover and Burn Severity Maps

The delineated watershed extent was acquired from the USGS Streamflow Statistics and Spatial Analysis Tools (StreamStats), (https://streamstats.usgs.gov/ss/). The land cover map for the study area were derived from the 2016 National Land Cover Database (NLCD), (http://www.mrlc.gov/). The burned severity map was obtained from Monitoring Trends in Burn Severity (MTBS), (http://www.mtbs.gov/).

4. RESULTS AND DISCUSSION

4.1. Pre-fire Model Calibration

The watershed models were developed with infiltration, surface roughness, and soil moisture. The pre-model calibration was prepared as an event-based simulation that included the 2018 January 9 atmospheric rainfall event. The return period of the event was of 200 to 500 years, implicating a high flow. The source of parametric values based on the Arroyo Seco watershed (Pradhan and Floyd, 2021) was employed due to its proximity to the Santa Barbara watershed. Infiltration average values considered for the pre-fire condition was based on the literature from Pradhan and Floyd, (2021) and GSSHA manual (Table 5).

Average parameter values for Manning's roughness were considered from the 2016 National Landover Database (NLCD) the Pradhan and Floyd (2021) and GSSHA defined values and study shown in Table 6. Initial soil moisture was assumed to be uniform across the watershed with value of 0.18.

Table 5. Pre-fire soil infiltration parameter values based on soil texture for San Ysidro model. (Amended: Pradhan and Floyd, 2021).

Soil infiltration parameter	Value
Saturated hydraulic conductivity (cm/h)	0.81
Capillary head (cm)	11.0
Porosity (m^3/m^3)	0.41
Pore distribution index (cm/cm)	0.37
Residual point (m^3/m^3)	0.04
Field capacity (m^3/m^3)	0.2
Wilting point (m^3/m^3)	0.09

Table 6. Pre-fire Manning's roughness parameter values for the routing model. (Amended: Pradhan and Floyd, 2021).

Land Cover Type/ Condition	Manning's roughness value ($s/m^{1/3}$)
Open Water	0.09
Developed, Open Space	0.15

Developed, Low Intensity	0.15
Developed, Medium Intensity	0.15
Deciduous Forest	0.45
Evergreen Forest	0.45
Mixed Forest	0.45
Shrub/ Scrub	0.44
Grassland/ Herbaceous	0.43
Pasture/Hay	0.20
Cultivated Crops	0.20
Woody Woodlands	0.14

4.2 Post-fire Model Calibration

On Table 7, the post-fire manning's roughness is reduced based on the post-fire burn condition (Pradhan and Floyd, 2021). Burn severity analyses of satellite coverage data showed that 11% of the area within the burn boundary were unburned, 31% burned with low severity, 56% moderately burned, and 1% burned with high severity. The most common type of burn in the San Ysidro Creek watershed was a medium burn, therefore Manning's roughness is taken as 0.18. Table 8 demonstrates the changed Manning's roughness values according to the burn severity. Soil moisture for was assumed to be uniform across the watershed at 0.13. Infiltration parameters changed within the model structure simulations according to the Pradhan and Floyd (2021) post-fire condition equation.

Table 7. Post-fire burn condition for infiltration model. (Amended: Pradhan and Floyd, 2021).

Burned Condition	**Manning Roughness Value ($s/m^{1/3}$)**
No burn	No Change
Low burn	0.2
Medium burn	0.18
High burn	0.15

Table 8. Post-fire Manning's roughness values for infiltration model. (Amended: Pradhan and Floyd, 2021).

Land Cover Condition	Manning's roughness value ($s/m^{1/3}$)
Deciduous/Evergreen/Mixed Forest + Medium Burn	0.18
Shrub + Medium Burn	0.18
Grassland + Medium Burn	0.18
Open Water	0.09
Developed, Open Space	0.15
Developed, Low Intensity	0.15
Developed, Medium Intensity	0.15
Deciduous Forest	0.45
Evergreen Forest	0.45
Mixed Forest	0.45
Shrub/ Scrub	0.44
Grassland/ Herbaceous	0.43
Pasture/Hay	0.20
Cultivated Crops	0.20
Woody Woodlands	0.14

4.3 Parameter Transfer Results for San Ysidro Creek

Figures 10 to 12 illustrate the GSSHA simulated discharge for pre- and post-fire conditions for San Ysidro Creek with transferred parameters from the Arroyo Seco watershed (Pradhan and Floyd, 2021). The soil moisture is estimated at 30-m resolution to match the GSSHA model grid resolution. The hydrological models were developed with infiltration, surface roughness, and soil moisture. In this study, three scenarios were modeled with the 09 January 2018 rainfall event; (a) the pre-fire condition without considering the fire effects,

underestimating the discharge (Figure 10), (b) the post-fire routing condition developed with a change in surface roughness (Figure 11), (c) the post-fire infiltration condition with a reduction factor of 0.1 (or 90% reduction) in soil hydraulic conductivity (Figure 12). Surface roughness and hydraulic conductivity were reduced according to the burn severity (Pradhan and Floyd, 2021). The purpose of modeling the pre-fire condition was to compare the resulting flood depth to the post-fire conditions to examine the effectiveness of the post-fire reduction factor. The difference between the three models is visually shown south of the watershed with spreading of the flood grid and in max flow depth increasing values. Figure 13 demonstrates the visual similarities between the observed and simulated depths.

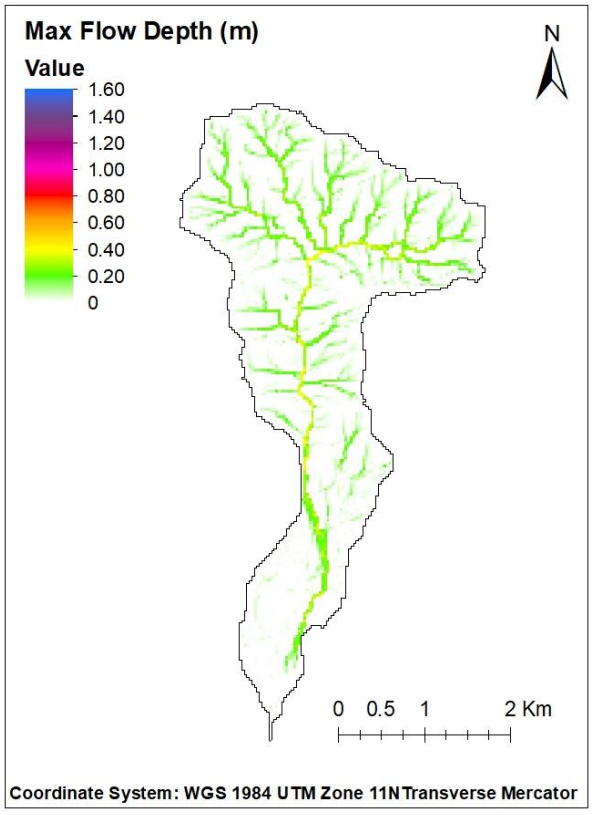

Figure 10. Pre-fire condition without considering the fire effects.

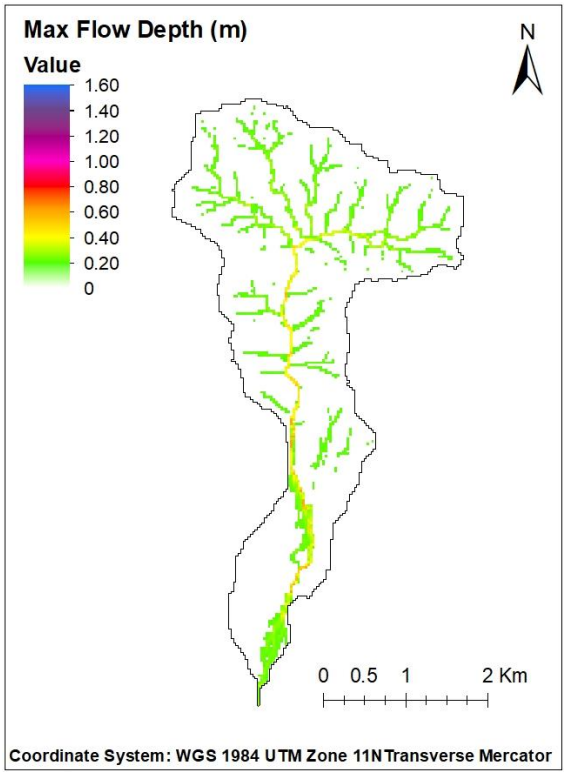

Figure 11. Post-fire routing condition developed with change in surface roughness.

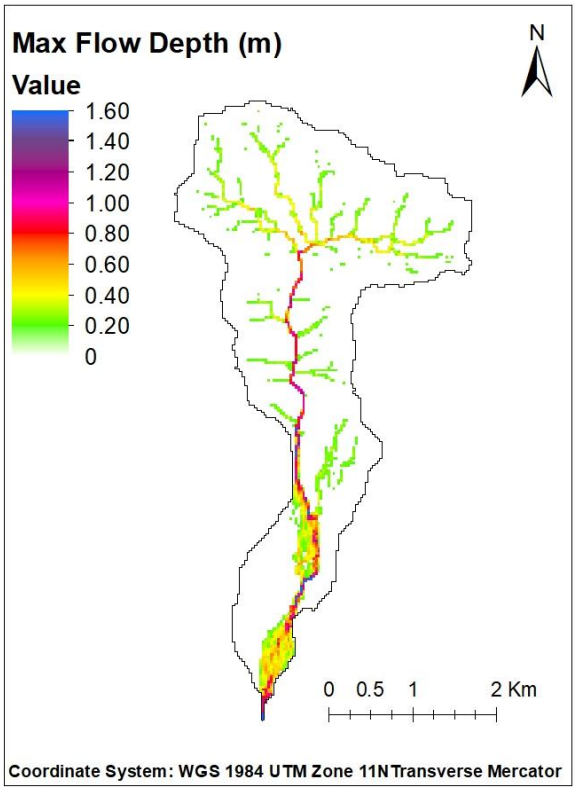

Figure 12. Post-fire infiltration condition with a reduction in soil hydraulic conductivity.

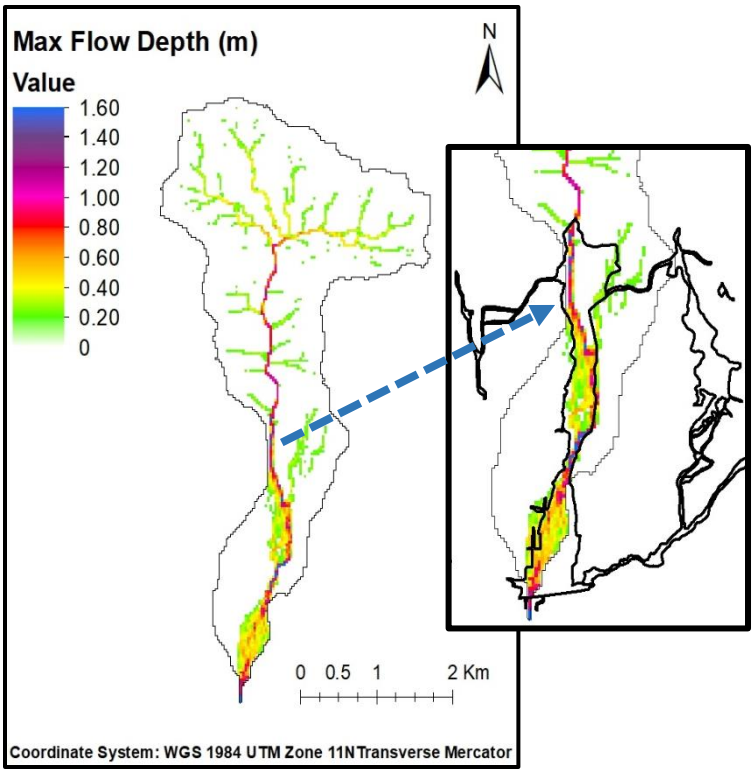

Figure 13. Post-fire infiltration condition with observed debris flows.

The illustrations of the different scenarios demonstrate the difference in flood surface elevations where the pre-fire condition has a maximum flow depth of 0.39 meters (Figure 10), the post-fire routing condition, 0.64 meters (Figure 11), and the post-fire infiltration condition, 1.60 meters (Figure 12). Figure 13 shows the simulated model results and the observed inundation boundaries outlined in black. It can be seen that the maximum flow depth increases by an order of magnitude between Figure 11 and 12 showing that a reduction in hydraulic conductivity increases flood surface elevations by an order of magnitude, implying that the runoff generation process is more significant than the routing process in this study.

Different flood depth values were extracted from various locations across the watershed and compared between observed and simulated depths (Figure 14). The observed values were from a small sample size of the entire watershed and then simulated based on the post-fire reduction condition. There is a cluster of points near the origin and one point outside of the

range. Future research should include more values from low to high ranges to better define trends.

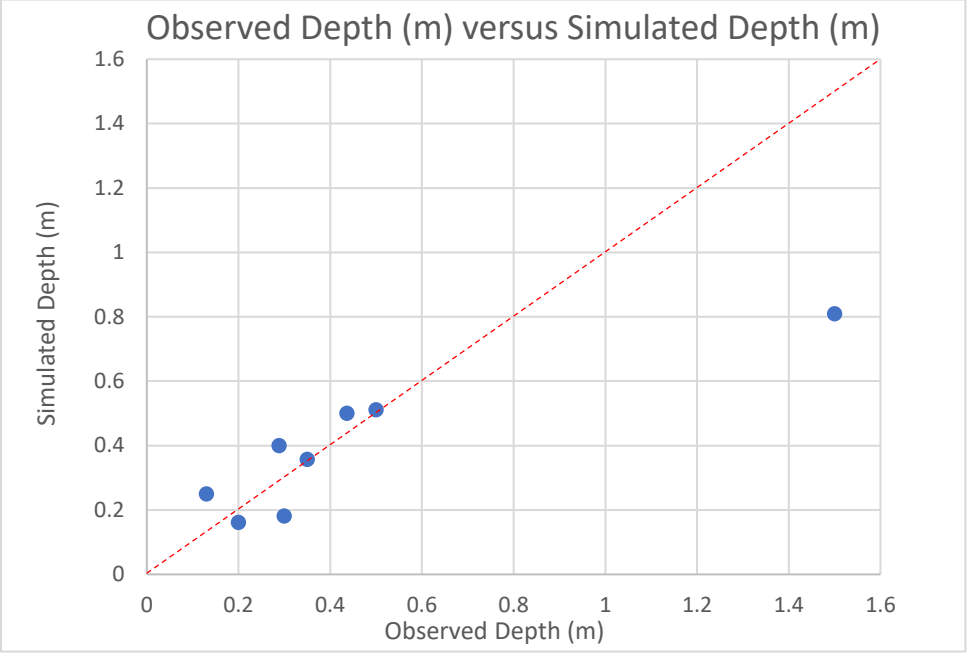

Figure 14. Observed depth versus simulated depth for the San Ysidro Creek of 09 January 2018 flows.

Based on the Pradhan and Floyd (2021) study, the hydraulic conductivity reduction factor was modeled with a 0.1 (or 90% reduction) and the coefficient of determination (R^2) used as the objective function between the observed and simulated values. Donigian (2002) affirms that the coefficient of determination (R^2) values range for assessing flows is to be very good when it is greater than 0.8; good when it is between 0.7 and 0.8; fair when it is between 0.6 and 0.7; and poor when it is less than 0.06. The post-fire reduction factor scenario had an R^2=0.79, and RMSE=0.26 and are considered satisfactory in model performance. The small sample size of observational flow depth values indicates that set of parameters identified were able to represent the hydrological processes.

4.4 Optimization Results for San Ysidro Creek

Hydraulic Conductivity and Manning's roughness were optimized using the SCE method with RMSE as the objective function and it was revealed that the hydrologic response was comparable to the transferred parameters.

4.4.1 Hydraulic Conductivity

As shown in Figure 15, the hydraulic conductivity reduction factor, Rf_k, was calibrated using the SCE optimization algorithm, RMSE was used as the objective function between the observed and simulated values.

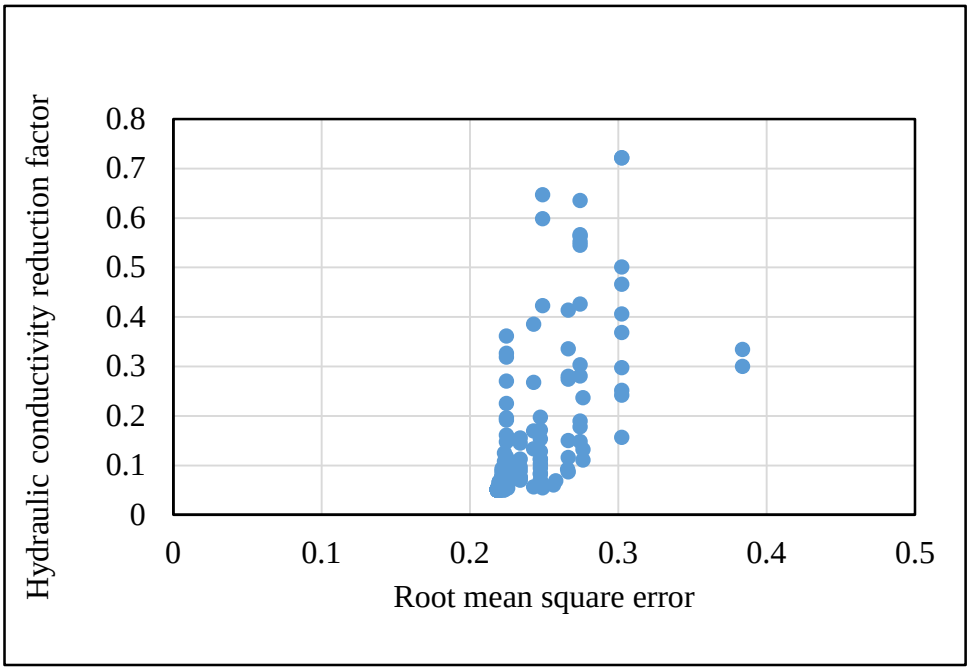

Figure 15. Hydraulic Conductivity Reduction Factor (Rf_k) versus Root Mean Square Error (RMSE) optimization based on SCE optimization algorithm.

Arroyo Seco was calibrated with an Rf_k equivalent to 0.10 (or 90% reduction) which is similar to the calibrated results for San Ysidro Creek. Figure 12 illustrates the relationship between the RMSE and the post-fire hydraulic conductivity reduction factor (Rf_k). In this post-fire scenario, the Rfk is equivalent to a 0.05 (or 95% reduction) in hydraulic conductivity, where

RMSE reaches an equilibrium between 0.2 and 0.3 demonstrating the impact of the fire on the land cover. Generally, the closer the RMSE is to 0, the more accurate the model is. The RMSE is comparable to that of the transferred parameters, reiterating that there was a reduction in hydraulic conductivity.

A study done by the USGS assessed core samples with tension infiltrometer measurements showed significant decreases in field hydraulic conductivity in burned areas relative to unburned areas therefore confirming the reduction in hydraulic conductivity results of this study (Ebel and Moody, 2020). The infiltration rate is a function of hydraulic conductivity, implicating that less water is infiltrating, therefore causing higher flow depths. The heating of organic matter in medium severity burns may be attributed to water repellency. Sorptivity directly relates water repellency to infiltration (Shillito et al., 2020).

4.4.2 Manning's Roughness

Manning's roughness, n, was calibrated using the SCE optimization algorithm, the root mean square error (RMSE) was used as the objective function between the observed and simulated values (Figure 16).

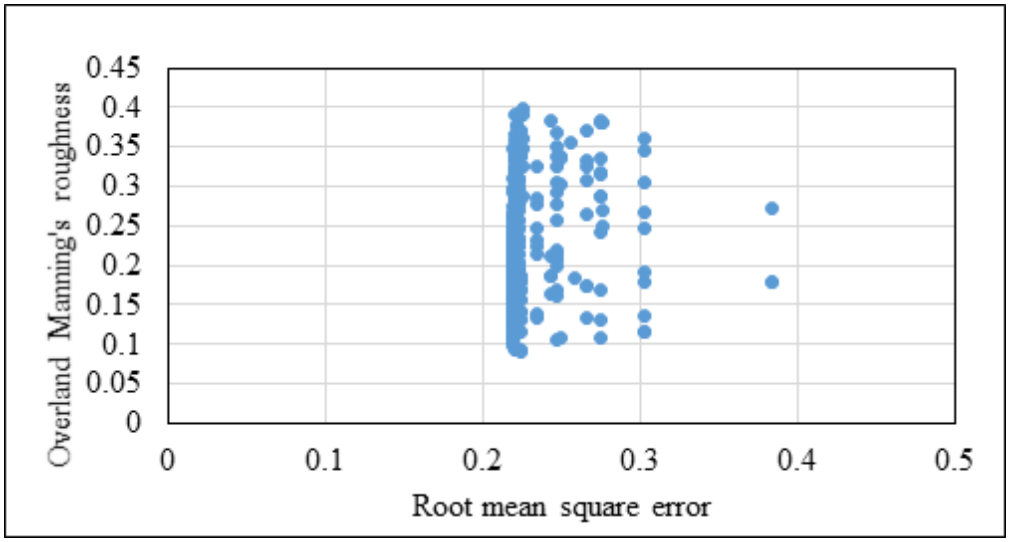

Figure 16. Manning's roughness versus Root Mean Square Error (RMSE) optimization based on SCE optimization algorithm.

Manning's roughness was considered for shrub land cover with ranges from 0.09 to 0.45. The RMSE has a cluster of points from 0.2 to 0.4, with a concentration of points at 0.22. There is not much sensitivity in manning's roughness as there was in the Rf_k. Surface roughness may change after a wildfire by the consumption of vegetation, litter, and duff, and by the deposition of an ash layer (Moody et al., 2013). The non-uniformity in the spatial distribution of sediment sources can change the transport process (Santi et al., 2008). Essentially, material and ashes can move with water causing changes in runoff patterns and sediment transport. Change in land cover is a dynamic process after fires, which may indicate surface roughness being a less sensitive parameter. Furthermore, the steep terrain and riprap stability may be factors to consider when computing hydraulic conditions. Manning's roughness is highly dependent on the flow depth/mean size of bed particle. The change in Manning's roughness from a very shallow depth (e.g., water depth is of same magnitude as mean size of bed particle) to not shallow depths (e.g., flow depth/mean size of bed particle > 30) can be of an order of magnitude (Brown and Clyde, 1989).

Similarity in both transferred and optimized parameters improved calibration and reduced the level of uncertainty in simulation runs. The San Ysidro Creek and Arroyo Seco watersheds had similar conditions and therefore had similar hydrologic responses following intense wildfire events. The parameterization methodology in this study can be further applied for ungauged or poorly gauged watersheds.

4.5 Assumptions and Limitations

The stream gages near San Ysidro Creek were burned during the Thomas fire, hence the lack of flood elevations and discharge datasets for the pre- and post-fire flood event. The maximum flow depth, h, was estimated from the run-up on the downstream side of trees and mudlines on structures acquired from the Kean et al. (2019) study. Measurements of soil-hydraulic properties were unavailable, therefore alternative methods were used for parameterization. Parameters from the Arroyo Seco watershed were first calibrated using the Nash-Sutcliffe efficiency as the objective function for pre- and post-fire events. Then, parameters were transferred using the calibrated values and calibrated once again using RMSE as an objective function.

5. CONCLUSION AND RECOMMENDATIONS

The hydrologic behavior of the San Ysidro Creek watershed was simulated using GSSHA after different scenarios (pre- and post-fire conditions) with transferred parameters from a similar, nearby watershed. The different scenarios accounted for the following identified parameters: Manning's roughness and the hydraulic conductivity reduction factor. Performing the model validation demonstrated a good representation of the observed data. Auto-calibration was then performed using the SCE method for both parameters and it was found the hydrologic response was comparable between the transferred parameters and auto-calibration. It was

established that although both parameters were sensitive, the hydraulic conductivity reduction factor was significantly more dominant.

Understanding hydrological processes in the development of pre-fire and post-fire models is crucial for emergency assessment. This study provided an organized physics-based framework that characterized different hydrological processes and provided a methodology for future studies for ungauged and poorly gauged watersheds.

Future research should focus on enhancing the understanding of post-fire soil hydraulic responses and modeling capabilities by improving post-fire field measurements to help validate models. Attention should be devoted to soil and land data collection as the data is important in characterizing post-fire hydrology. Since wildfires are increasing in frequency, multiple methods of field measurements including remote sensing should be explored in the years that follow. Laboratory tests on hydraulic conductivity and manning's roughness could provide a parametric range for future studies.

Additional studies on Manning's roughness should be applied to test for uncertainty. Likewise, routing conditions with similar topography should be considered. An assessment of the extent of similarity in parameter transfer should be evaluated to understand when parameter transfer is appropriate. Finally, GSSHA can be implemented for planning structural designs in flood-prone areas for communities to be protected.

REFERENCES

Abebe, N. A., Ogden, F. L., & Pradhan, N. R. (2010). Sensitivity and uncertainty analysis of the conceptual HBV rainfall–runoff model: Implications for parameter estimation. Journal of Hydrology, 389(3-4), pp. 301-310.

Addison, P., Oommen, T. (2020). Post-fire debris flow modeling analyses: case study of the post-Thomas Fire event in California. Nat Hazards 100, pp. 329–343. https://doi.org/10.1007/s11069-019-03814-x

Barnhart, K. R., Jones, R. P., George, D. L., McArdell, B. W., Rengers, F. K., Staley, D. M., & Kean, J. W. (2021). Multi-model comparison of computed debris flow runout for the 9 January 2018 Montecito, California post-wildfire event. Journal of Geophysical Research: Earth Surface, 126, e2021JF006245.

Beven, K.J., Binley, A. (1992). The future of distributed models: model calibration and uncertainty prediction. Hydrologic Process. 6, pp. 279–298.

Beven, K. J. (2000a). Uniqueness of place and process representations in hydrological modelling, Hydrologic Earth Systems Science, 4, pp. 203–213.

Bodí, M. B., Martin, D. A., Balfour, V. N., Santín, C., Doerr, S. H., Pereira, P., ... & Mataix-Solera, J. (2014). Wildland fire ash: production, composition and eco-hydro-geomorphic effects. Earth-Science Reviews, 130, pp. 103-127.

Brown, S. A., Clyde, E. S. (1989). Design of riprap revetment (No. FHWA-IP-89-016). United States. Federal Highway Administration.

Cannon, S. H., Gartner, J. E., Wilson, R. C., Bowers, J. C., Laber, J. L. (2008). Storm rainfall conditions for floods and debris flows from recently burned areas in southwestern Colorado and southern California. Geomorphology, 96(3-4), pp. 250-269.

Cannon S., DeGraff J. (2009). The Increasing Wildfire and Post-Fire Debris-Flow Threat in Western USA, and Implications for Consequences of Climate Change.

Chen, Li, Berli, Markus, and Chief, Karletta. (2013). Examining Modeling Approaches for the Rainfall-Runoff Process in Wildfire-Affected Watersheds: Using San Dimas Experimental Forest. Journal of the American Water Resources Association (JAWRA) 49 (4): pp. 851– 866. DOI: 10.1111/jawr.12043.

Cunge, J. A. (1969). On the Subject of a Flood Propagation Computation Method (Muskingum Method). Journal of Hydraulic Research, Vol. 7, No. 2, pp. 205-230.

DeBano, L. F. (1991). The effect of fire on soil properties. In Proceedings management and productivity of western-Montane. Forest Soils, pp. 151-155.

Dooge, J. C. I. (2003). Linear theory of hydrologic systems EGU Reprint Series. European Geosciences Union, 1-327.

Donigian, A.S. (2002). Watershed model calibration and validation: The HSPF experience. In TMDLS Conference 2002. Water Environment Federation, pp. 44-73.

Downer, C.W.; Ogden, F.L. (2006) Gridded Surface Subsurface Hydrologic Analysis (GSSHA) User's Manual, Version 1.43 for Watershed Modeling System 6.1; ERDC/CHL SR-06-1; System Wide Water Resources Program, Coastal and Hydraulics Laboratory, U.S. Army Corps of Engineers, Engineer Research and Development Center: Vicksburg, MS, USA.

Duan, Q., Gupta, V.K., Sorooshian, S. (1992). Effective and efficient global optimization for conceptual rainfall–runoff models. Water Resources Research. 28 (4), pp.1015–1031.

Elliot, W.J., Hall, D.E., Robichaud, P.R. (2010). FS Peak Flow Calculator. Version 2010.10.28. U.S. Department of Agriculture, Forest Service, Rocky Mountain Research Station, Moscow, ID.

Feyen, L. & Vázquez, R. & Christiaens, Karen & Sels, O. & Feyen, (2000). Application of a distributed physically-based hydrological model to a medium size catchment. Hydrology and Earth System Sciences. 4. pp. 47-63. 10.5194/hess-4-47-2000.

Floyd, I.E. (2021). Non-Newtonian Model Development for Post-Wildfire Flood Risk Management. LSU Doctoral Dissertations. 5513.

Ebel, B.A., Moody, J.A., and Martin, D.A., (2012). Hydrologic conditions controlling runoff generation immediately after wildfire. Water Resources Research, v. 48, pp. 1-13

Ebel, BA, Moody, JA. (2020). Parameter estimation for multiple post-wildfire hydrologic models. Hydrological Processes; 34: pp. 4049– 4066.

Ebrahimian, A, Sample-Lord, K, Wadzuk, B, Traver, R. (2020). Temporal and spatial variation of infiltration in urban green infrastructure. Hydrological Processes; 34: pp.1016–1034.

Green, W.H. and G. Ampt. (1911). Studies of soil physics, part I – the flow of air and water through soils. Journal of Agricultural Science. 4: pp. 1-24.

Hawkins, R.H. and A.B. Munoz, (2011). Wildcat5 for Windows (W5W): Documentation and Manual. School of Natural Resources and Environment. University of Arizona, Tucson, Arizona.

J.L. Florsheim, E.A. Keller, D.W. (1991). Best Fluvial sediment transport in response to moderate storm flows following chaparral wildfire, Ventura County, southern California. Geological Society of America Bulletin, 103 pp. 504-511.

John, A., Fuentes, H. R., & George, F. (2021). Characterization of the water retention curves of Everglades wetland soils. Geoderma, 381, 114724.

Jones, J. A. A. (1997). Global Hydrology: Processes, Resources and Environmental Management, Chapter 6, Modelling Runoff Processes.

Kean, J. W., Staley, D. M., Lancaster, J. T., Rengers, F. K., Swanson, B. J.,Coe, J. A., Lindsay, D. N. (2019). Inundation, flow dynamics, and damage in the 9 January 2018

Montecito debris-flow event, California, USA: Opportunities and challenges for post-wildfire risk assessment. Geosphere, 15(4), pp. 1140–1163.

Keeley, J. E. (2009). Fire intensity, fire severity and burn severity: a brief review and suggested usage. International journal of wildland fire, 18(1), pp. 116-126.

Kinoshita, A. M., Hogue, Terri S., and N., Carolyn, (2014). Evaluating Pre- and Post-Fire Peak Discharge Predictions across Western U.S. Watersheds. Journal of the American Water Resources Association (JAWRA) 50 (6): pp. 1540- 1557. DOI: 10.1111/jawr.12226

Lane, P.N.J., Sheridan, G.J., Noske, P.J. (2006). Changes in sediment loads and discharge from small mountain catchments following wildfire in south eastern Australia. Journal of Hydrology 331, pp. 495-510.

Latron, J., Gallart, F. (2008). Runoff generation processes in a small Mediterranean research catchment (Vallcebre, Eastern Pyrenees). Journal of Hydrology. 358. pp. 206-220. 10.1016/j.jhydrol.2008.06.014.

Leon A. S.**,** Kanashiro E. A., and Gonzalez-Castro J. A. (2013), Fast Approach for Unsteady Flow Routing in Complex River Networks Based on Performance Graphs, ASCE Journal of Hydraulic Engineering, 139(3), pp. 284–295.

Lopes, A. R., Girona-García, A., Corticeiro, S., Martins, R., Keizer, J. J., and Vieira, D. C. S. (2021). What is wrong with post-fire soil erosion modelling? A meta-analysis on current approaches, research gaps, and future directions. Earth Surface Process. Landforms, 46: 205– 219. https://doi.org/10.1002/esp.5020.

Madsen, H., (2000). Automatic calibration of a conceptual rainfall–runoff model using multiple objectives. Journal of Hydrology. 235, pp. 276–288.

Malone, R. W., Yagow, G., Baffaut, C., Gitau, M. W., Qi, Z., Amatya, D. M., ... & Green, T. R. (2015). Parameterization guidelines and considerations for hydrologic models. Transactions of the ASABE, 58(6), pp. 1681-1703.

Martin, D.A. and Moody, J.A. (2001). Comparison of soil infiltration rates in burned and unburned mountainous watersheds. Hydrologic Processes, 15: pp. 2893-2903.

Miller M. (ed.). (1994). Fire Effects Guide. NFES 2394/PMS 481. National Wildfire Coordinating Group, National Interagency Fire Center: Boise, ID; II-12.

Moody, J.A., Martin, D.A., Haire, S.L., Kinner, D.A. (2008a). Linking runoff response to burn severity after wildfire. Hydrological Processes 22, pp. 2063–2074.

Moody, J.A., Shakesby, R.A., Robichaud, P.K., Cannon, S.H., Martin, D.A., (2013). Current research issues related to post-wild wildfire runoff and erosion processes. Earth-Science Reviews 122, pp. 10-37.

Napper, C., (2010). BAER Hydrology Model Questionnaire Results, USDA, Forest Service Technology and Development Center, San Dimas, California.

Parson, A., Robichaud, PR., Lewis, SA., Napper, C, Clark, JT. (2010). Field guide for mapping post-fire soil burn severity. Gen. Tech. Rep. RMRS-GTR-243. Fort Collins, CO: U.S. Department of Agriculture, Forest Service, Rocky Mountain Research Station. pp. 49. doi: 10.2737/RMRS-GTR-243

Paudel, B. R., Udawatta, R. P., Kremer, R. J., & Anderson, S. H. (2012). Soil quality indicator responses to row crop, grazed pasture, and agroforestry buffer management. Agroforestry Systems, 84(2), pp. 311-323.

Pradhan, N. R., F. L. Ogden, Y. Tachikawa, and K. Takara. (2008). Scaling of slope, upslope area, and soil water deficit: Implications for transferability and regionalization in topographic index modeling, Water Resources Research., pp. 44, W12421, doi:10.1029/2007WR006667.

Pradhan NR, Floyd I. (2021). Event Based Post-Fire Hydrological Modeling of the Upper Arroyo Seco Watershed in Southern California. Water 13(16):2303.

Jian, M., Berli, M., & Ghezzehei, T. A. (2018). Soil structural degradation during low-severity burns. Geophysical Research Letters, 45, pp. 5553–5561. https://doi.org/10.1029/2018GL078053

Julien, P.Y., Saghafian, B. and Ogden, F.L. (1995). Raster-based Hydrologic Modeling of Spatially varied surface runoff. JAWRA Journal of the American Water Resources Association, 31: pp. 523-536.

Refsgaard, J. C., & Storm, B. (1990). Construction, calibration and validation of hydrological models. In distributed hydrological modelling. Springer, Dordrecht. pp. 41-54.

Rice, R. M. (1974). The hydrology of chaparral soils, in Proceedings, Symposium on Living with the Chaparral: Riverside, California, Sierra Club, pp. 27-34.

Rowe, P.B., C.M. Countryman, and H.C. Storey, (1949). Probably Peak Discharge and Erosion Rates from Southern California Watersheds as Influenced by Fire. Department of Agriculture, Forest Service, Pacific Southwest Forest and Range Experiment Station, Berkeley, California.

Santi, P.M., dewolf, V.G., Higgins, J.E., Cannon, S.H., Gartner, J.E., (2008). Sources of debris flow material in burned areas. Geomorphology 96, pp. 310–321.

Scott, K. M., & Williams, R. P. (1978). Erosion and sediment yields in the Transverse Ranges, southern California (Vol. 1030). US Government Printing Office.

Shillito, R. M., Berli, M., & Ghezzehei, T. A. (2020). Quantifying the effect of subcritical water repellency on sorptivity: A physically based model. Water Resources Research, 56, e2020WR027942. https://doi.org/10.1029/2020WR027942=

Spear, R.C., Hornberger, G.M., (1980). Eutrophication in peel inlet, II, identification of critical uncertainties via generalized sensitivity analysis. Water Resources Research 14, pp. 43–49.

State of California. (2018). Thomas Fire Final Report, CA-VNC-103156. State of California Watershed Emergency Response Team. Sacramento, CA: State of California.

Tindall, J. A., Kunkel, J. R., & Anderson, D. E. (1999). Unsaturated zone hydrology for scientists and engineers (Vol. 4). Upper Saddle River, NJ: Prentice Hall.

Ward, A. S., Gooseff, M. N., & Johnson, P. A. (2011). How can subsurface modifications to hydraulic conductivity be designed as stream restoration structures? Analysis of Vaux's conceptual models to enhance hyporheic exchange. Water Resources Research, 47(8).

U.S. Army Corps of Engineers, (2010). Hydrologic Modeling System HEC-HMS: User's Manual version 3.5. Institute for Water Resources, Hydrologic Engineering Center, Davis, California.

U.S. Department of Agriculture, Soil Conservation Service, (1991). Engineering Field Handbook: Chapter 2 – Estimating Runoff. In: National Engineering Handbook, H.M. Kautz, J.A. Aull, R.C. Barnes, K.H. Beauchamp, T.B. Chambers, R.L. Fox, and J.W. Haas (Editors). Soil Conservation Service: Part 650. U.S. Department of Agriculture, Washington, D.C.

Vrugt, J. A., Gupta, H. V., Bouten, W., and Sorooshian, S. (2003). A Shuffled Complex Evolution Metropolis algorithm for optimization and uncertainty assessment of hydrologic model parameters, Water Resources Research, 39, pp. 1201.

Wagener, T., Sivapalan, M., Troch, P. and Woods, R. (2007). Catchment Classification and Hydrologic Similarity. Geography Compass, 1, pp. 901-931.

Winter, T. C. (2001). The concept of hydrologic landscapes. Journal of the American Water Resources Association, 37, pp. 335–349.

Zema, D.A. (2021). Postfire management impacts on soil hydrology. Current Opinion in Environmental Science & Health, pp. 100252.

APPENDICES

APPENDIX A

Rainfall Data Inputs for Pre- and Post-fire Conditions

EVENT "Event of 08 January 2018- rainfall stops on 10 January"

NRGAG 3

NRPDS 72

COORD 262750.0 3811227.0 "Summerland raingage #1"

COORD 257366.0 3812722.0 "Montecito raingage #2"

COORD 264301.0 3815903.0 "Doulton Tunnel raingage #3"

RATES 2018 01 08 00 00 0.000 0.000 0.000

RATES 2018 01 08 01 00 0.000 0.254 0.000

RATES 2018 01 08 02 00 0.000 0.000 0.000

RATES 2018 01 08 03 00 0.000 0.000 0.000

RATES 2018 01 08 04 00 0.000 0.000 0.000

RATES 2018 01 08 05 00 0.000 0.000 0.000

RATES 2018 01 08 06 00 0.000 0.000 0.000

RATES 2018 01 08 07 00 0.000 0.000 0.000

RATES 2018 01 08 08 00 0.000 0.000 0.000

RATES 2018 01 08 09 00 0.000 0.000 0.000

RATES 2018 01 08 10 00 0.000 0.000 0.000

RATES 2018 01 08 11 00 0.250 0.000 0.000

RATES 2018 01 08 12 00 0.750 0.508 1.016

RATES 2018 01 08 13 00 0.750 0.000 0.508

RATES 2018 01 08 14 00 0.750 1.016 1.016

RATES 2018 01 08 15 00 0.760 0.508 1.016

RATES 2018 01 08 16 00 0.750 1.524 3.302

RATES 2018 01 08 17 00 1.270 0.762 3.048

RATES 2018 01 08 18 00 0.250 1.524 1.778

RATES 2018 01 08 19 00 0.250 0.000 0.000

RATES 2018 01 08 20 00 0.250 0.000 0.000

RATES 2018 01 08 21 00 0.250 0.254 0.762

RATES 2018 01 08 22 00 0.250 0.508 0.254

RATES 2018 01 08 23 00 0.250 0.000 0.000

RATES 2018 01 09 00 00 0.250 0.000 0.000

RATES 2018 01 09 01 00 0.250 0.254 1.778

RATES 2018 01 09 02 00 1.270 4.064 3.556

RATES 2018 01 09 03 00 22.100 21.336 29.464

RATES 2018 01 09 04 00 11.430 7.366 17.018

RATES 2018 01 09 05 00 2.540 2.540 3.556

RATES 2018 01 09 06 00 0.250 0.762 1.016

RATES 2018 01 09 07 00 2.290 1.270 2.540

RATES 2018 01 09 08 00 1.150 0.254 0.508

RATES 2018 01 09 09 00 0.000 0.254 0.000

RATES 2018 01 09 10 00 8.890 3.810 8.636

RATES 2018 01 09 11 00 1.270 0.254 3.048

RATES 2018 01 09 12 00 0.250 0.762 5.842

RATES 2018 01 09 13 00 0.250 0.254 0.000

RATES 2018 01 09 14 00 0.000 0.000 1.016

RATES 2018 01 09 15 00 0.000 0.000 0.000

RATES 2018 01 09 16 00 0.500 3.810 0.000

RATES 2018 01 09 17 00 0.000 0.000 0.000

RATES 2018 01 09 18 00 0.250 0.000 0.000

RATES 2018 01 09 19 00 0.250 0.000 0.000

RATES 2018 01 09 20 00 0.250 0.000 0.000

RATES 2018 01 09 21 00 0.000 0.254 0.000

RATES 2018 01 09 22 00 0.000 0.000 0.000

RATES 2018 01 09 23 00 0.000 0.000 0.000

RATES 2018 01 10 00 00 0.000 0.000 0.000

RATES 2018 01 10 01 00 0.000 0.000 0.000

RATES 2018 01 10 02 00 0.000 0.000 0.000

RATES 2018 01 10 03 00 0.000 0.000 0.000

RATES 2018 01 10 04 00 0.000 0.000 0.000

RATES 2018 01 10 05 00 0.000 0.000 0.000

RATES 2018 01 10 06 00 0.000 0.000 0.000

RATES 2018 01 10 07 00 0.000 0.000 0.000

RATES 2018 01 10 08 00 0.000 0.000 0.254

RATES 2018 01 10 09 00 0.000 0.000 0.000

RATES 2018 01 10 10 00 0.000 0.000 0.000

RATES 2018 01 10 11 00 0.000 0.000 0.000

RATES 2018 01 10 12 00 0.000 0.000 0.000

RATES 2018 01 10 13 00 0.250 0.000 0.000

RATES 2018 01 10 14 00 0.250 0.000 0.000

RATES 2018 01 10 15 00 0.250 0.000 0.000

RATES 2018 01 10 16 00 0.250 0.000 0.000

RATES 2018 01 10 17 00 0.250 0.000 0.000

RATES 2018 01 10 18 00 0.250 0.000 0.000

RATES 2018 01 10 19 00 0.000 0.000 0.000

RATES 2018 01 10 20 00 0.000 0.000 0.000

RATES 2018 01 10 21 00 0.000 0.000 0.000

RATES 2018 01 10 22 00 0.000 0.000 0.000

RATES 2018 01 10 23 00 0.000 0.000 0.000

APPENDIX B

Pre-fire Project File

```
GSSHAPROJECT
WMS WMS 11.1.10 (64-bit)
WATERSHED_MASK          "San_Ysidro_pre_fire.msk"
PROJECT_PATH            ""
#LandSoil               "San_Ysidro_pre_fire.lsf"
NON_ORTHO_CHANNELS
FLINE                   "San_Ysidro_pre_fire.map"
METRIC
GRIDSIZE                30.000000
ROWS                    247
COLS                    119
TOT_TIME                5000
TIMESTEP                10
OUTROW                  247
OUTCOL                  36
OUTSLOPE                0.001000
MAP_FREQ                30
HYD_FREQ                30
MAP_TYPE                1
ELEVATION               "San_Ysidro_pre_fire.ele"
DEPTH                   "San_Ysidro_pre_fire.dep"
FLOOD_GRID              "San_Ysidro_pre_fire.gfl"
OVERTYPE                ADE
INF_REDIST
#INDEXGRID_GUID         "landuse.idx"
#INDEXGRID_GUID         "uniform.idx"
```

#INDEXGRID_GUID "burnt_map_from_nawa.idx"
MAPPING_TABLE "San_Ysidro_pre_fire.cmt"
SUMMARY "San_Ysidro_pre_fire.sum"
OUTLET_HYDRO "San_Ysidro_pre_fire.otl"
PRECIP_FILE "San_Ysidro_pre_fire.gag"
RAIN_INV_DISTANCE

Appendix C

Pre-fire Roughness, Infiltration, and Soil Moisture Inputs

GSSHA_INDEX_MAP_TABLES

INDEX_MAP "landuse"

INDEX_MAP "uniform"

INDEX_MAP "burnt_map "

ROUGHNESS "landuse"

NUM_IDS 12

ID	DESCRIPTION1	DESCRIPTION2	ROUGH
11	Roughness ID		0.090000
21	Roughness ID		0.150000
22	Roughness ID		0.150000
23	Roughness ID		0.150000
41	Roughness ID		0.450000
42	Roughness ID		0.450000
43	Roughness ID		0.450000
52	Roughness ID		0.440000
71	Roughness ID		0.430000
81	Roughness ID		0.200000
82	Roughness ID		0.200000
90	Roughness ID		0.140000

GREEN_AMPT_INFILTRATION "landuse"

NUM_IDS 12

ID	DESCRIPTION1	DESCRIPTION2	HYDR_COND	CAPIL_HEAD	POROSITY	PORE_INDEX	RESID_SAT	FIELD_CAPACITY	WILTING_PT
11	Infiltration ID		0.810000	11.000000	0.410000	0.370000	0.040000	0.200000	0.090000
21	Infiltration ID		0.810000	11.000000	0.410000	0.370000	0.040000	0.200000	0.090000
22	Infiltration ID		0.810000	11.000000	0.410000	0.370000	0.040000	0.200000	0.090000
23	Infiltration ID		0.810000	11.000000	0.410000	0.370000	0.040000	0.200000	0.090000
41	Infiltration ID		0.810000	11.000000	0.410000	0.370000	0.040000	0.200000	0.090000
42	Infiltration ID		0.810000	11.000000	0.410000	0.370000	0.040000	0.200000	0.090000
43	Infiltration ID		0.810000	11.000000	0.410000	0.370000	0.040000	0.200000	0.090000
52	Infiltration ID		0.810000	11.000000	0.410000	0.370000	0.040000	0.200000	0.090000
71	Infiltration ID		0.810000	11.000000	0.410000	0.370000	0.040000	0.200000	0.090000
81	Infiltration ID		0.810000	11.000000	0.410000	0.370000	0.040000	0.200000	0.090000
82	Infiltration ID		0.810000	11.000000	0.410000	0.370000	0.040000	0.200000	0.090000
90	Infiltration ID		0.810000	11.000000	0.410000	0.370000	0.040000	0.200000	0.090000

GREEN_AMPT_INITIAL_SOIL_MOISTURE "uniform"

NUM_IDS 1

ID	DESCRIPTION1	DESCRIPTION2	SOIL_MOISTURE
1	Soil moisture ID		0.180000

APPENDIX D

Post-fire Project File

```
GSSHAPROJECT
WMS WMS 11.1.5 (64-bit)
WATERSHED_MASK          "GSSHAModel_post_fire_routing.msk"
PROJECT_PATH            ""
#LandSoil               "GSSHAModel_post_fire_routing.lsf"
#PROJECTION_FILE        "GSSHAModel_post_fire_routing_prj.pro"
NON_ORTHO_CHANNELS
FLINE                   "GSSHAModel_post_fire_routing.map"
METRIC
GRIDSIZE                30.000000
ROWS                    247
COLS                    119
TOT_TIME                5000
TIMESTEP                10
OUTROW                  247
OUTCOL                  36
OUTSLOPE                0.001000
MAP_FREQ                30
HYD_FREQ                30
MAP_TYPE                1
ELEVATION               "GSSHAModel_post_fire_routing.ele"
DEPTH                   "GSSHAModel_post_fire_routing.dep"
FLOOD_GRID              "GSSHAModel_post_fire_routing.gfl"
OVERTYPE                ADE
INF_REDIST
#INDEXGRID_GUID         "landuse.idx"
```

```
#INDEXGRID_GUID         "uniform.idx"
#INDEXGRID_GUID         "burnt_map_from_nawa.idx"
#INDEXGRID_GUID         "Combine.idx"
#INDEXGRID_GUID         "lu_burn_combo_nawa.idx"
MAPPING_TABLE           "GSSHAModel_post_fire_routing.cmt"
SUMMARY                 "GSSHAModel_post_fire_routing.sum"
OUTLET_HYDRO            "GSSHAModel_post_fire_routing.otl"
PRECIP_FILE             "GSSHAModel_post_fire_routing.gag"
RAIN_INV_DISTANCE
IN_CELLDEPDIS_LOCATION      "in_celldepdis_file.txt"
OUT_CELLDEPDIS_LOCATION  "out_celldepdis_file.txt"
POSTFIRE                        "burnt_map.idx" 0.10
```

Appendix E

Post-fire Roughness, Infiltration, and Soil Moisture Inputs

GSSHA_INDEX_MAP_TABLES

INDEX_MAP "landuse"

INDEX_MAP "uniform"

INDEX_MAP "burnt_map "

INDEX_MAP "lu_burn_combo "

ROUGHNESS "lu_burn_combo"

NUM_IDS 15

ID	DESCRIPTION1	DESCRIPTION2	ROUGH
1	Roughness ID		0.130000
2	Roughness ID		0.130000
3	Roughness ID		0.130000
11	Roughness ID		0.090000
21	Roughness ID		0.150000
22	Roughness ID		0.150000
23	Roughness ID	r	0.150000
41	Roughness ID		0.450000
42	Roughness ID		0.450000
43	Roughness ID		0.450000
52	Roughness ID		0.440000
71	Roughness ID		0.430000
81	Roughness ID		0.200000
82	Roughness ID		0.200000
90	Roughness ID		0.140000

GREEN_AMPT_INFILTRATION "Combined"

NUM_IDS 12

ID DESCRIPTION1 DESCRIPTION2 HYDR_COND CAPIL_HEAD POROSITY PORE_INDEX RESID_SAT FIELD_CAPACITY WILTING_PT

1 0.810000 11.000000 0.410000 0.370000 0.040000 0.200000 0.090000

2 Land ID #21, Untitled landuse 0.810000 11.000000 0.410000 0.370000 0.040000 0.200000 0.090000

3 Land ID #43, Untitled landuse 0.810000 11.000000 0.410000 0.370000 0.040000 0.200000 0.090000

4 Land ID #42, Untitled landuse 0.810000 11.000000 0.410000 0.370000 0.040000 0.200000 0.090000

5 Land ID #71, Untitled landuse 0.810000 11.000000 0.410000 0.370000 0.040000 0.200000 0.090000

6 Land ID #11, Untitled landuse 0.810000 11.000000 0.410000 0.370000 0.040000 0.200000 0.090000

7 Land ID #22, Untitled landuse 0.810000 11.000000 0.410000 0.370000 0.040000 0.200000 0.090000

8 Land ID #41, Untitled landuse 0.810000 11.000000 0.410000 0.370000 0.040000 0.200000 0.090000

9 Land ID #23, Untitled landuse 0.810000 11.000000 0.410000 0.370000 0.040000 0.200000 0.090000

10 Land ID #90, Untitled landuse 0.810000 11.000000 0.410000 0.370000 0.040000 0.200000 0.090000

11 Land ID #82, Untitled landuse 0.810000 11.000000 0.410000 0.370000 0.040000 0.200000 0.090000

12 Land ID #81, Untitled landuse 0.810000 11.000000 0.410000 0.370000 0.040000 0.200000 0.090000

GREEN_AMPT_INITIAL_SOIL_MOISTURE "Combined"

NUM_IDS 12

ID DESCRIPTION1 DESCRIPTION2 SOIL_MOISTURE

1 Land ID #52, Untitled landuse 0.130000

2 Land ID #21, Untitled landuse 0.130000

3 Land ID #43, Untitled landuse 0.130000

4 Land ID #42, Untitled landuse 0.130000

5 Land ID #71, Untitled landuse 0.130000

6	Land ID #11, Untitled landuse	0.130000
7	Land ID #22, Untitled landuse	0.130000
8	Land ID #41, Untitled landuse	0.130000
9	Land ID #23, Untitled landuse	0.130000
10	Land ID #90, Untitled landuse	0.130000
11	Land ID #82, Untitled landuse	0.130000
12	Land ID #81, Untitled landuse	0.130000

VITA

FRANCISCA OLMOS DE AGUILERA

Born, Santiago, Chile

2015-2020	B.S., Environmental Engineering Florida International University Miami, Florida
2019	First Place in Environmental Competition of the American Society of Civil Engineers (ASCE) Southeastern Conference Water Environment Federation (WEF) Inflow Program Recipient
2019-2020	Fundraising Director of Engineers Without Borders (EWB) Marketing Chair of Water Environmental Federation (WEF) Secretary of Society of Women Engineers (SWE)
2021	Florida Section of the American Water Works Association (FSAWWA) Roy Likins Scholarship Recipient
2021-2022	Treasurer of Engineers Without Borders (EWB)
2021-2022	ERDC-CHL Fellow Graduate Research Assistant Florida International University Miami, Florida

PUBLICATIONS AND PRESENTATIONS

Olmos de Aguilera, F., Pradhan, N.R., Fuentes, H.R., Floyd, I.E., Cagle, T.S. (2023) (*In Progress*) An Analysis of the 9 January 2018 Montecito, California Post-fire Runoff Event Using GSSHA Hydrological Model. Paper to be presented at SEDHYD Conference in St. Louis, Missouri.